NASA CR-137842
MDC E1415 VOL. I

NASA CONTRACTOR
REPORT

NASA CR-137842
MDC E1415 VOL. I

(NASA-CR-137842) PLANETARY/DOD ENTRY TECHNOLOGY FLIGHT EXPERIMENTS. VOLUME 1: EXECUTIVE SUMMARY Final Report, 1 Apr. 1975 - 29 Feb. 1976 (McDonnell-Douglas Astronautics Co.) 57 p HC $4.50 CSCL 22A G3/13

N76-28243

Unclas
47940

PLANETARY/DoD ENTRY TECHNOLOGY FLIGHT EXPERIMENTS

Executive Summary

By H.E. Christensen, R.J. Krieger, W.R. McNeilly and H.C. Vetter

Prepared by

MCDONNELL DOUGLAS ASTRONAUTICS COMPANY — EAST

St. Louis, Missouri 63166 (314) 232-0232

for Ames Research Center

NATIONAL AERONAUTICS AND SPACE ADMINISTRATION • WASHINGTON, D.C. • FEBRUARY 1976

NASA CR-137842
MDC E1415 VOL. I
29 FEBRUARY 1976

PLANETARY/DoD ENTRY TECHNOLOGY FLIGHT EXPERIMENTS

COPY NO. 12

Executive Summary

By H.E. Christensen, R.J.Krieger,
W.R. McNeilly and H.C. Vetter

Prepared Under Contract No. NAS 2–8678 by

MCDONNELL DOUGLAS ASTRONAUTICS COMPANY – EAST

Saint Louis, Missouri

for

NATIONAL AERONAUTICS AND SPACE ADMINISTRATION

FOREWORD

This final report was prepared by McDonnell Douglas Astronautics Company-East (MDAC-E) for NASA Ames Research Center Contract NAS2-8678, Planetary/DoD Entry Technology Flight Experiments. It covers the period 1 April 1975 to 29 February 1976. This effort was performed for the National Aeronautics and Space Administration, Ames Research Center, under the direction of the Thermal Protection Branch with Dr. Phillip R. Nachtsheim as Contract Technical Monitor and with the cooperation of Capt. R. J. Callahan of SAMSO and R. C. Loesch of Aerospace Corporation as advisors for the DoD portion of the study.

The report consists of four volumes:

- Volume I - Executive Summary
- Volume II - Planetary Entry Flight Experiments
- Volume III - Planetary Entry Flight Experiments Handbook
- Volume IV - DoD Entry Flight Experiments

List of Pages

INTRODUCTION

The objective of this program was to determine the feasibility of using Shuttle to launch planetary and DoD entry flight experiments. The results of the program are presented in two parts: (1) simulating outer planet environments during an earth entry test, the prediction of Jovian and earth radiative heating dominated environments, mission strategy, booster performance and entry vehicle design, and (2) the DoD entry test needs for the 1980's, the use of Shuttle to meet these DoD test needs, modifications of test procedures as pertaining to using Shuttle, modifications to Shuttle to accommodate DoD test missions and the unique capabilities of Shuttle. The major findings of this program are summarized in this volume.

PLANETARY ENTRY FLIGHT EXPERIMENTS

PLANETARY ENTRY FLIGHT EXPERIMENTS

The overall conclusion arising from this portion of the study is that the Shuttle and its upper stage can provide the high speed earth entry conditions needed for useful simulation of outer planet environments on a full size, probe shaped vehicle. Furthermore, candidate heat shield concepts can be developed as well as intense environments measured to expand scientific knowledge of entry physics.

The planetary technology objectives of a Shuttle-launched earth entry flight test program are summarized on Figure 1. Shock layer radiation measurements are necessary to calibrate computational prediction techniques. Experiments to assess radiation blockage are necessary to derive design correlations which cannot be obtained by ground tests. These first two phenomena determine the net radiative heat transfer to the heat shield. Thermochemical decomposition of carbon phenolic is well understood. However, mechanical erosion in severe planetary heating environments cannot be predicted without representative data, data that cannot be obtained in ground tests. Th performance and structural integrity of the reflective heat shield concept can only be obtained by exposure to a representative entry environment. Additionally, the ever-present technology problems associated with boundary layer transition, turbulent heating, heating in separated flow regimes, etc. will also be subjects of experimentation. Of particular interest will be boundary layer behavior under conditions of massive ablation rates.

Even though the entry environments of radiative heating, convective heating, deceleration loads and surface pressures are severe, design provisions enable air recovery so that post flight examination can be made. The planetary entry flight experiment sequence is shown in Figure 2.

Radiative Heating Simulation is the Key Requirement - Compared with earth entry, outer planet entry is characterized by high entry velocity, high convective and radiative heat fluxes and relatively short entry time. The thermal environment of outer planet probes becomes increasingly dominated by shock layer radiation as entry velocity increases. In Figure 3 entry conditions and environment parameters for representative outer planet probe entries are shown along with values anticipated for the forthcoming Venus probe mission, as well as with values experienced in earth entry by project FIRE (the most energetic earth entry performed to date). It is seen that the outer planet heating environment is substantially greater than that expected for Venus and orders of magnitude more severe than earth flight experience.

PLANETARY ENTRY EXPERIMENTS

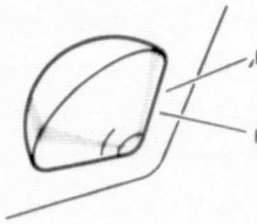

PRIMARY OBJECTIVES

HEATING ENVIRONMENT PREDICTION
- SHOCK LAYER RADIATION
- RADIATION BLOCKAGE BY ABLATION

HEAT SHIELD DESIGN
- CARBON PHENOLIC MECHANICAL EROSION
- SILICA PERFORMANCE AND STRUCTURAL INTEGRITY

OTHER OBJECTIVES

- BOUNDARY LAYER TRANSITION
- TURBULENT HEATING INFORMATION
- DECELERATION LOADS
- AFTERBODY HEATING
- HEAT SHIELD THERMAL STRESS
- VEHICLE AERODYNAMICS AND STABILITY

FIGURE 1

PLANETARY ENTRY SIMULATION MISSION

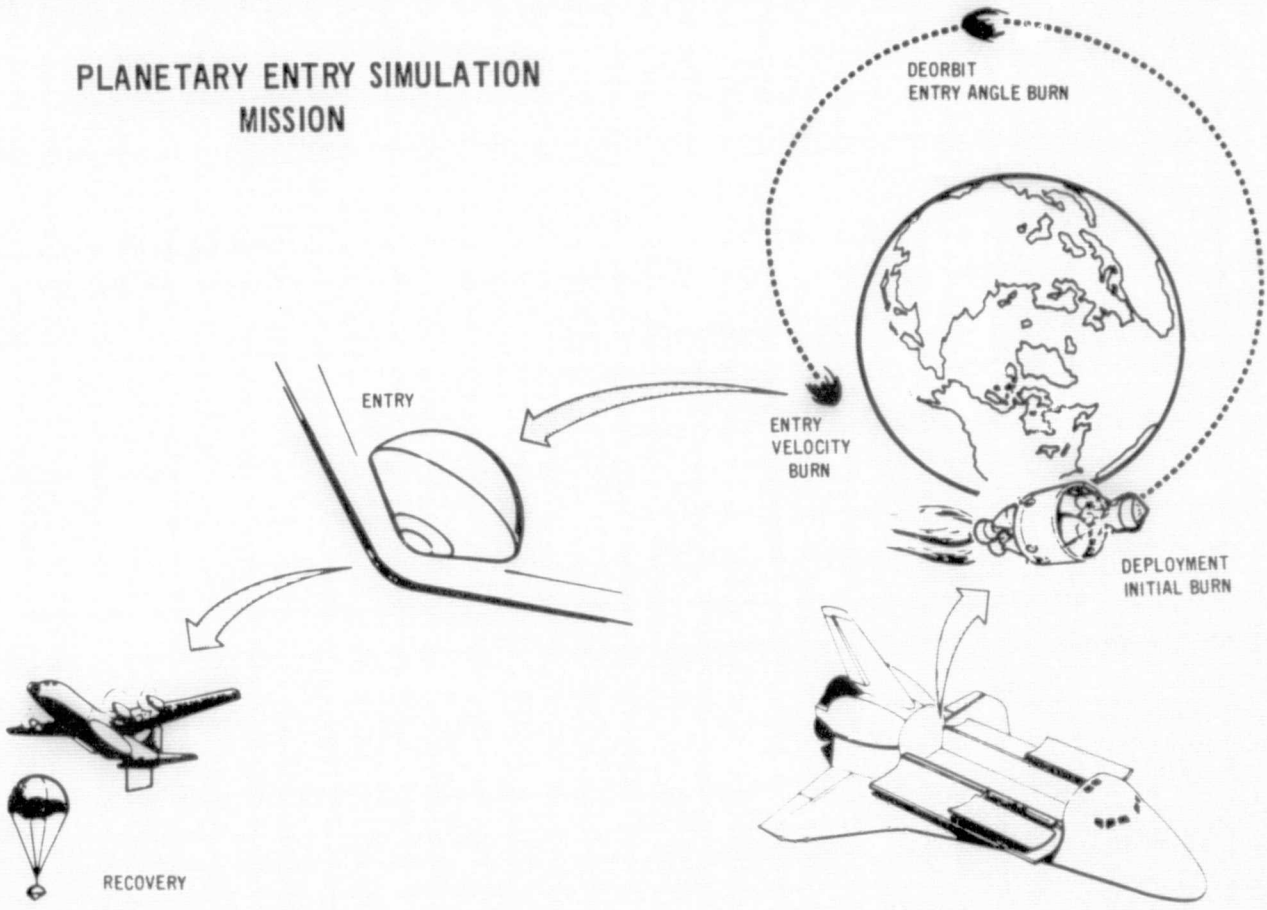

FIGURE 2

SIMULATION REQUIREMENTS SUMMARY

	OUTER PLANETS				VENUS (PIONEER/ VENUS 78)	EARTH (PROJECT FIRE)
	JUPITER	SATURN	URANUS			
ENTRY CONDITIONS (INERTIAL)						
VELOCITY (KM/SEC)	59.6	36.7	24.9		11.6	11.3
ANGLE (DEGREES)	−7.5	−40	−50		−20 TO −90	−15
ATMOSPHERE						
DESIGNATION	NOMINAL	COOL	NOMINAL	COOL	CO_2/N_2	AIR
MASS FRACTION (H_2 – He)	.75–.23	.55–.40	.65–.16	.20–.80		
ENVIRONMENT						
PEAK HEATING RATE (KW/CM^2)						
RADIATIVE	38	20.5	0	33	2 TO 5	0.4
CONVECTIVE	15	12.5	4	11	3 TO 5	0.7
TOTAL HEAT (KJ/CM^2)	440	74	31	80	14 TO 21	13
HEAT PULSE DURATION (SEC)	14	10	15	4	3 TO 11	40
PEAK STAGNATION PRESSURE (ATM)	8	12	8	18	7 TO 8	0.5
PEAK DECELERATION (G)	300	700	500	700	200 TO 500	85

FIGURE 3

The heating environment is also significantly affected by the atmosphere model chosen for analysis. Typically, a cool atmosphere model results in higher peak heating than either a nominal or warm model. The nominal atmosphere for Jupiter is used in light of recent Pioneer II flight data while the more conservative selection of a cool atmosphere is made for Saturn pending further information from the Pioneer II mission. Selection of a Uranus atmosphere model presents a special problem. The cool atmosphere, which results in high radiative rates of Jupiter proportions, is now considered invalid because of excessively high helium content relative to solar abundance. Use of a nominal atmosphere eliminates the radiative component altogether. Hence, for the present, the Uranus entry environment is assumed the same as Saturn.

Jovian entry environments were the most severe conditions and used more extensively to design the earth entry vehicle. As shown in Figure 4, radiative heating is about three times greater than convective. Uncertainties in Jovian entry angle (three degrees spread) results in a 58% increase in radiative heating and a 19% increase in convective heating. Adequate description of shock temperature, temperature distribution across the shock layer, and species concentration are also important in determining radiative heating with mass transfer (blowing). Figure 5 presents a summary description of these factors. Knowledge of the temperature dis-distribution across the shock layer is important to computing radiative heating. Both carbonaceous and hyperpure silica heat shields were analyzed for Jovian entry. Injection of ablation material into the shock layer further reduced radiative heating to the wall with carbon having the greatest reduction (46%), silica about 18%. However, due to silica's excellent reflectance, it had to accommodate far less heat: only 1.7 kW/cm^2 as compared to 9.1 kW/cm^2 for carbon. Testing of hyperpure and carbonaceous materials under simulated Jovian environments should be performed to substantiate these trends.

High Speed Earth Entries Needed to Simulate Radiative Heating Can Be Achieved - Outer planet radiative heating can be simulated during a high speed earth entry based on analysis of non-blowing, cooled and mass injected shock layers. Maps of attainable environments as a function of entry conditions, such as shown in Figure 6, were prepared to aid the experiment planner. Earth entry velocities much less than those of planetary entry are sufficient to simulate planetary heating because of atmosphere composition differences. The outer planet atmospheres are compared primarily of hydrogen-helium mixtures at about the solar abundance ratio,

JUPITER ENVIRONMENT

- o V_{REL} = 47 km/sec
- o ALT = 450 km
- o R_N = .22m
- o R_N/R_B = .50
- o STAGNATION POINT
- o NON BLOWING

RADIATIVE FLUX

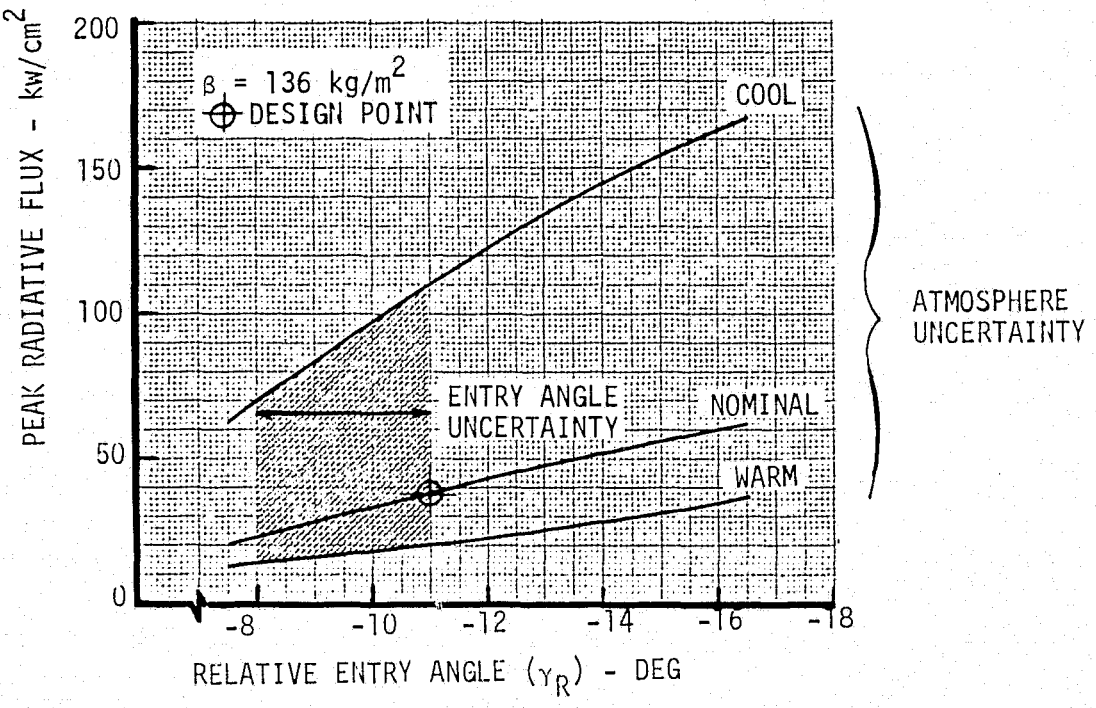

CONVECTIVE FLUX

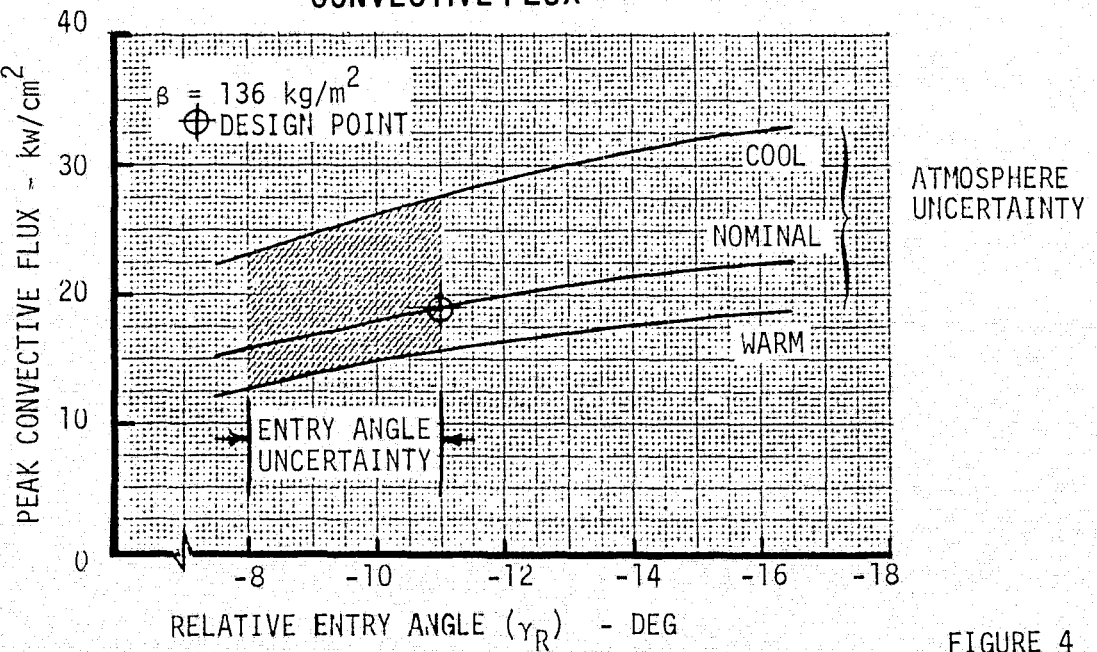

FIGURE 4

RADIANT HEATING COMPARISON OF SEVERAL INJECTANTS IN JUPITER ENTRY SHOCK LAYER

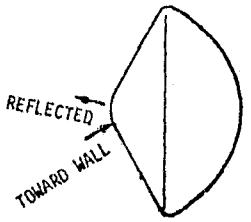

ATMOSPHERIC COMPOSITION (WEIGHT FRACTION)
HELIUM (He) 0.21
HYDROGEN (H_2) 0.79

T_S = 15947°K

P_S = 5.32 ATM

	FLUX TOWARD WALL (kW/cm^2)	FLUX AWAY FROM WALL (kW/cm^2)	NET FLUX TO ABLATOR (kW/cm^2)
NO INJECTANT	31.980		
SILICON (Si) INJECTION SILICA ABSORPTANCE T_W = 3450°K	21.853	21.477	0.376
SILICON (Si) INJECTION ABSORPTANCE = 0.5 T_W = 3450°K	21.853	11.332	10.521
SILICA (SiO_2) INJECTION SILICA ABSORPTANCE T_W = 3450°K	24.252	23.279	0.973
CARBON (C) INJECTION ABSORPTANCE = 0.8 T_W = 4564°K	13.810	4.730	9.080

FIGURE 5

EARTH ENTRY HEATING RATES

- o STAGNATION POINT
- o NON-BLOWING
- o INERTIAL ENTRY CONDITIONS
- o β = 120 kg/m^2
- o R_N = .22 m

(a) RADIATIVE FLUX

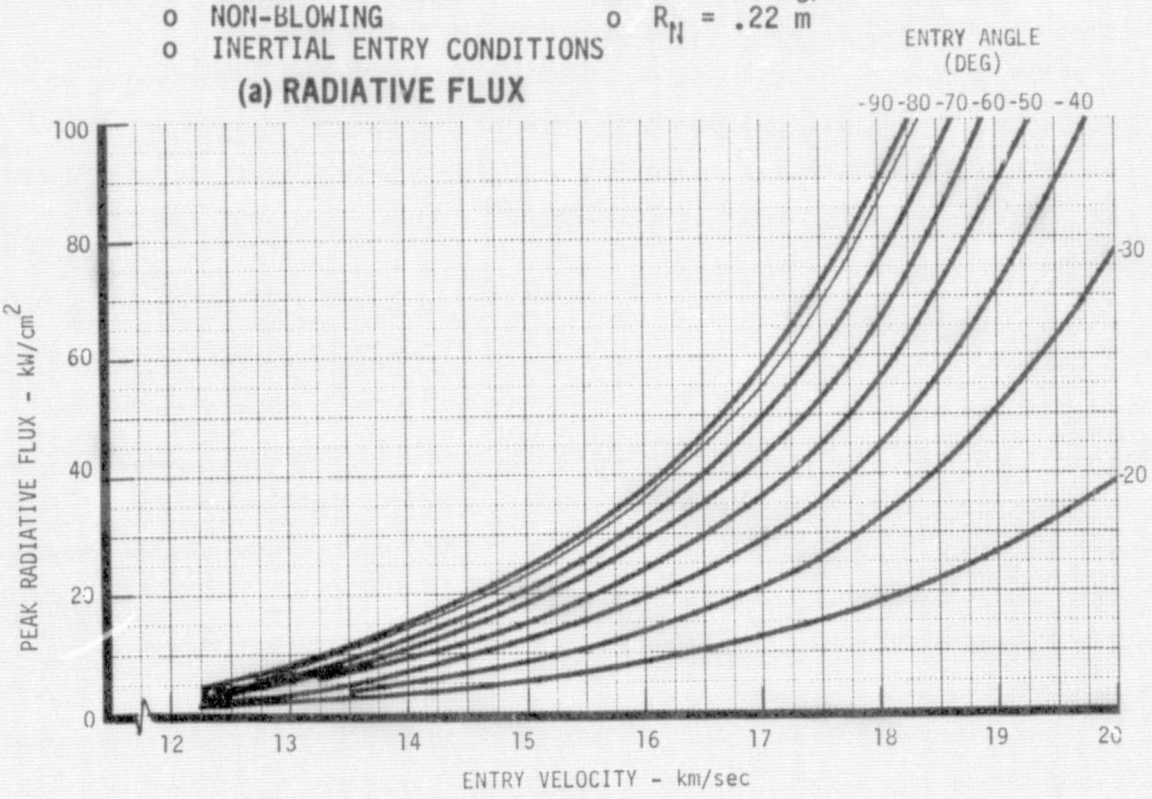

(b) CONVECTIVE FLUX

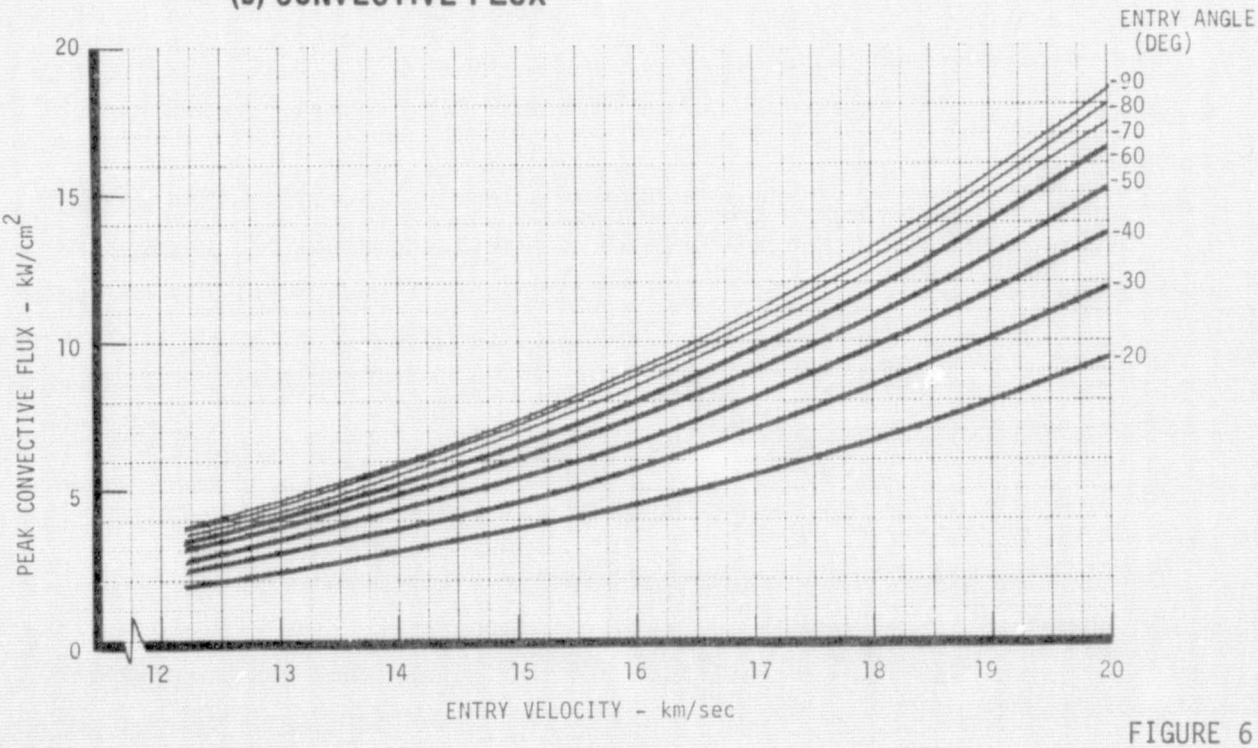

FIGURE 6

whereas the earth atmosphere is nearly 21 percent oxygen and 79 percent nitrogen. From basic thermodynamics it is known that the low molecular weight gases, hydrogen and helium,have a much higher heat capacity than air. Thus simulation of similar shock layer temperatures or heating rates in air require a much lower entry speed than that of planetary entries, which range from 25 km/sec for Uranus to 60 km/sec for Jupiter. The higher molecular weight of air also results in a steeper atmospheric density gradient which enhances simulation of the peak environment conditions but reduces the heating duration.

In order to achieve the high earth entry velocities required to simulate planetary entry conditions,both direct and lofted deorbit techniques after Space Shuttle deployment were examined. The direct entry maneuver required excessively high thrust levels to achieve high entry velocities from low earth orbit. Hence, a deorbit maneuver involving an intermediate transfer to higher altitudes was selected. This maneuver is shown schematically in Figure 7. The booster is placed into a circular earth orbit at about 300 km by the Shuttle and an initial burn is made for transfer to a higher altitude. The apoapsis will typically range from 2 to 10 earth radii. A second burn is performed at apoapsis to obtain the desired entry angle and begin the descent trajectory. Just prior to entry (120 km) a third burn is accomplished along the flight path to achieve a high entry velocity. Mission analyses indicated that the first burn would occur over the Pacific Ocean, the second, a burn at apoapsis, would occur over South American and radars at Ascension Test Range could track the entry vehicle during the entire descent including the final burn. The ground tracks are shown in Figure 8 for apoapsis altitudes of 3.0 and 6.5 earth radii.

Non-Blowing Radiative Flux Can be Simulated - High radiation flux levels of outer planet proportions can be achieved by earth entry flights using a variety of Shuttle launched boosters. This is illustrated by Figure 9 which summarizes the comparison of planetary simulation requirements with earth flight test booster capabilities. The shaded area of Figure 9 represents the earth entry conditions required to simulate the radiative flux level range of interest. The lower bound of 10 kW/cm^2 is the minimum level to produce a radiation dominated environment. The upper bound of 40 kW/cm^2 is the maximum design level for Jupiter entry simulation. The four booster classes presented represent the range of entry condition capability available from current technology upper stages. The example designs used for each class are the Centaur/TE364-4 (cryogenic), the Transtage/TE364-4

DEORBIT MANEUVER STRATEGY

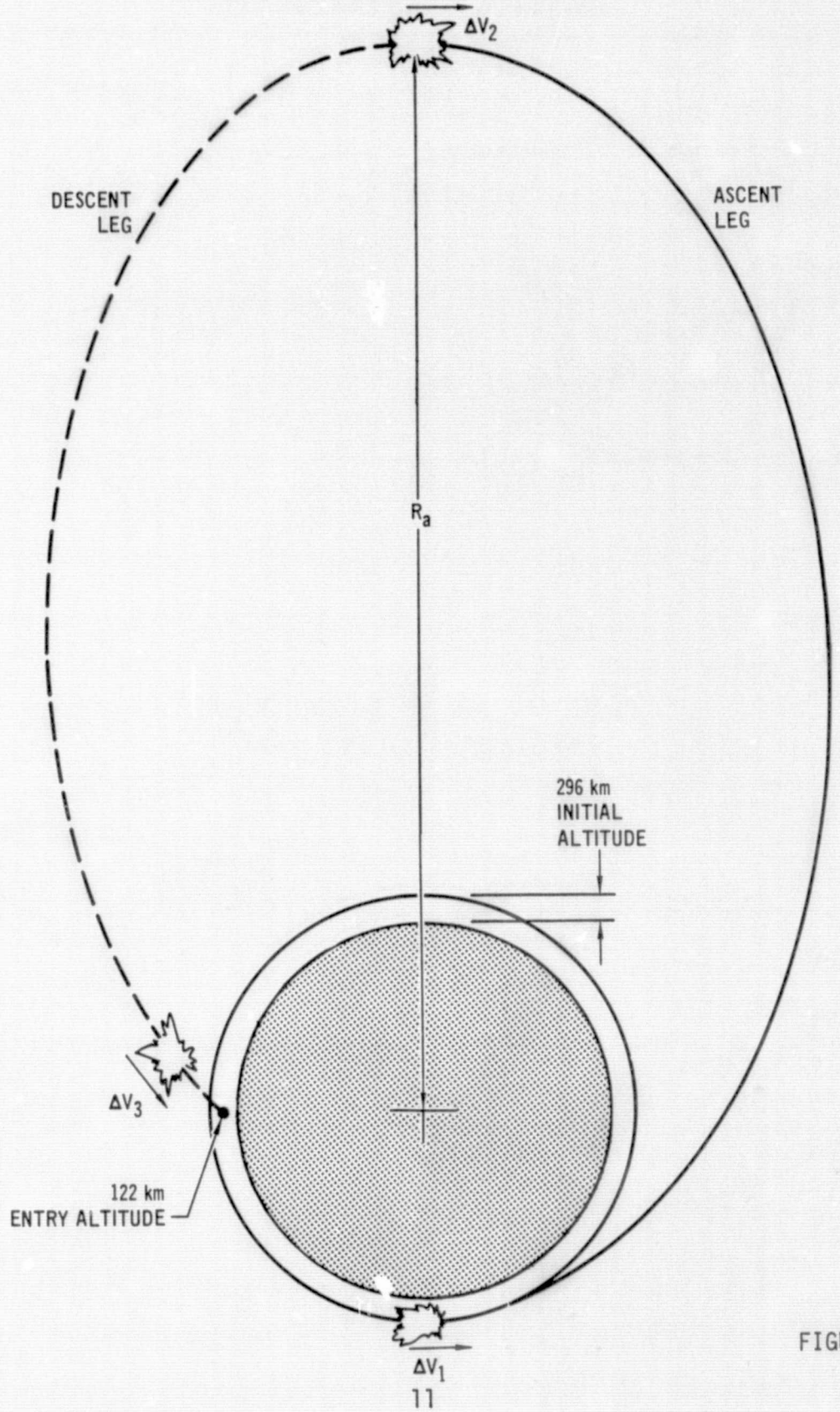

FIGURE 7

PLANETARY ENTRY GROUND TRACKS
(APOAPSIS = 6.5 EARTH RADII)

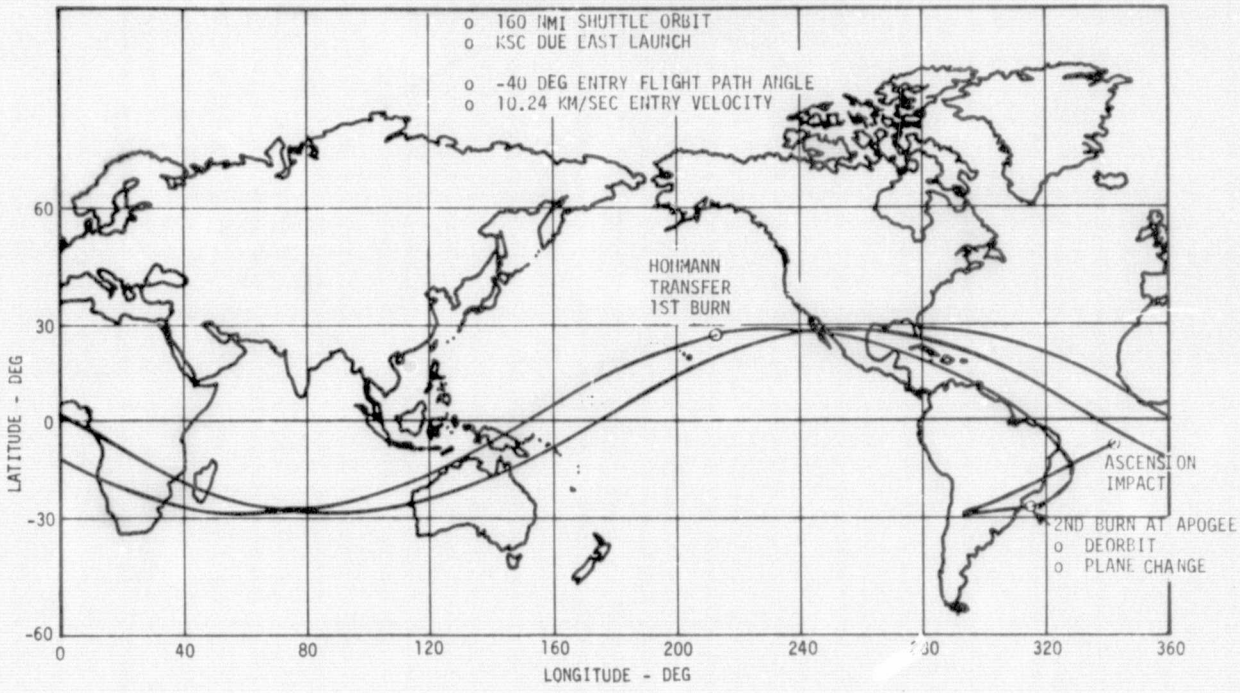

PLANETARY ENTRY GROUND TRACKS
(APOAPSIS = 3.0 EARTH RADII)

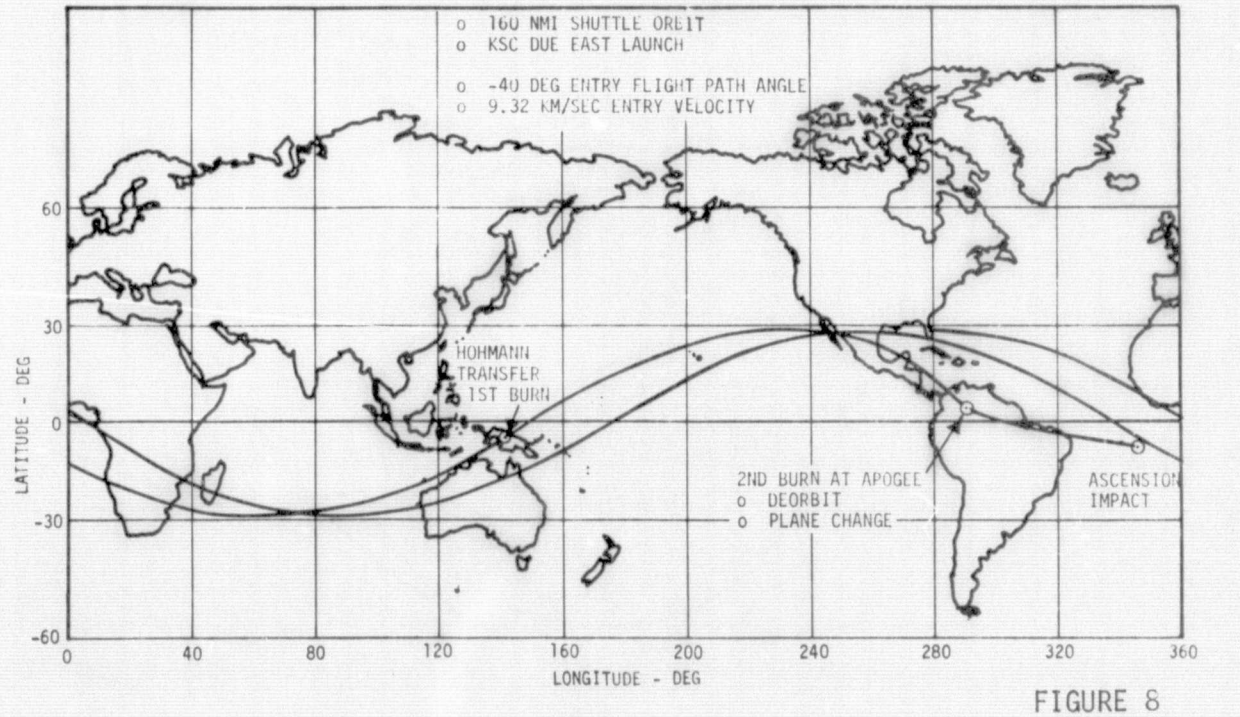

FIGURE 8

RADIATIVE FLUX SIMULATION CAPABILITY VS REQUIREMENTS

- o STAGNATION POINT
- o NON BLOWING
- o PAYLOAD = 100 kg
- o β = 120 kg/m^2
- o Ra = 10 EARTH RADII
- o IN PLANE MANEUVERS

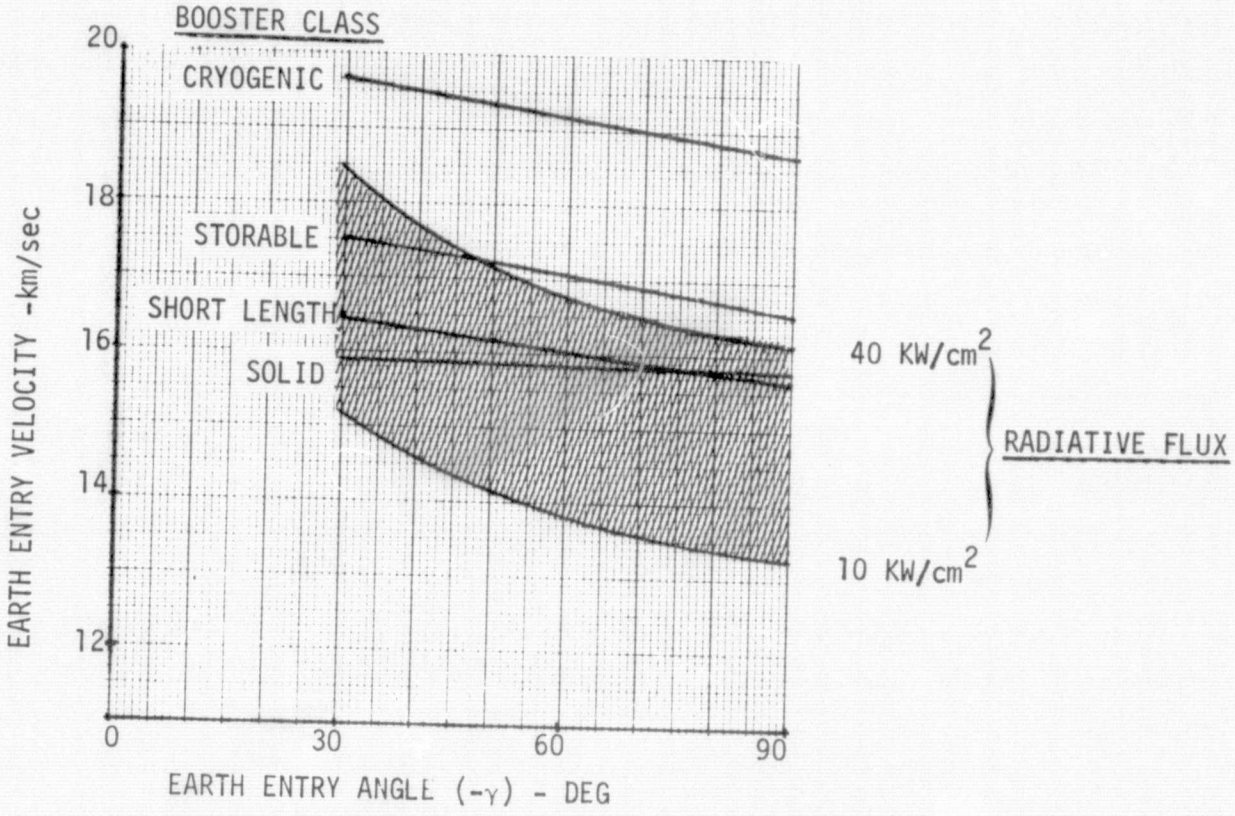

FIGURE 9

(storable), a Shuttle RCS Velocity Package (short length), and the IUS/TE364-4 (solid). As shown, the entry condition capability of each booster classes is well above the minimum requirement and, in fact, exceed the 20 kW/cm^2 maximum requirement for Saturn/Uranus entry simulation. Further, the capability of the cryogenic and storable classes exceed the maximum Jupiter requirement of 40 kW/cm^2.

A more detailed comparison that includes the effect of apoapsis altitude and entry vehicle mass variations is shown in Figure 10 using the Transtage/TE364-4 (storable class) as the booster example. One point to be noted is that increasing apoapsis altitude increases the peak radiative flux level that can be simulated with a given booster and entry vehicle mass. This effect is particularly pronounced at low apoapsis but reaches a point of diminishing returns at an apoapsis of about 10 earth radii. Hence for a fixed booster and entry vehicle, apoapsis altitude can be used to adjust the level of radiative flux produced during entry. For instance, a 100 kg entry vehicle (reference design) could simulate a Saturn entry at an $R_a = 2$ while the same mass vehicle could simulate a Jupiter entry by increasing R_a to about 6.5.

A second point illustrated by Figure 10 is that increasing entry vehicle mass actually improves radiative flux simulation capability if C_DA is held constant. In this case, the ballistic coefficient (m/C_DA) increases proportionally to the mass increase which causes a corresponding increase in radiative flux for the same entry conditions. Offsetting this is the reduced entry condition capability of the booster resulting from increased payload mass. However, the net effect is beneficial; the entry condition requirement for a given radiative flux level goes down faster than the booster entry condition capability. This can be seen in Figure 10 by noting that as payload mass increases, higher radiative flux levels are achievable if R_a is held constant or a lower R_a can be used if radiative flux is held constant.

Although earth entry conditions can be selected that will result in matching peak radiative flux levels for entry into Saturn or Jupiter, the simultaneous matching of all other entry parameters can only be approximated. Figure 11 presents four earth entry environment parameters as a function of the peak radiative heat flux. It is seen that peak convective heat flux is essentially independent of entry angle and always falls short of the planetary value by just under a factor of two. The total integrated heat load can be varied by about a factor of three depending on the selection of the entry angle. This permits one to

TRANSTAGE/TE364-4 RADIATIVE FLUX SIMULATION CAPABILITY

- o STAGNATION POINT
- o NON BLOWING
- o IN PLANE MANEUVERS
- o OPTIMUM ENTRY ANGLE

(a) APOAPSIS EFFECT

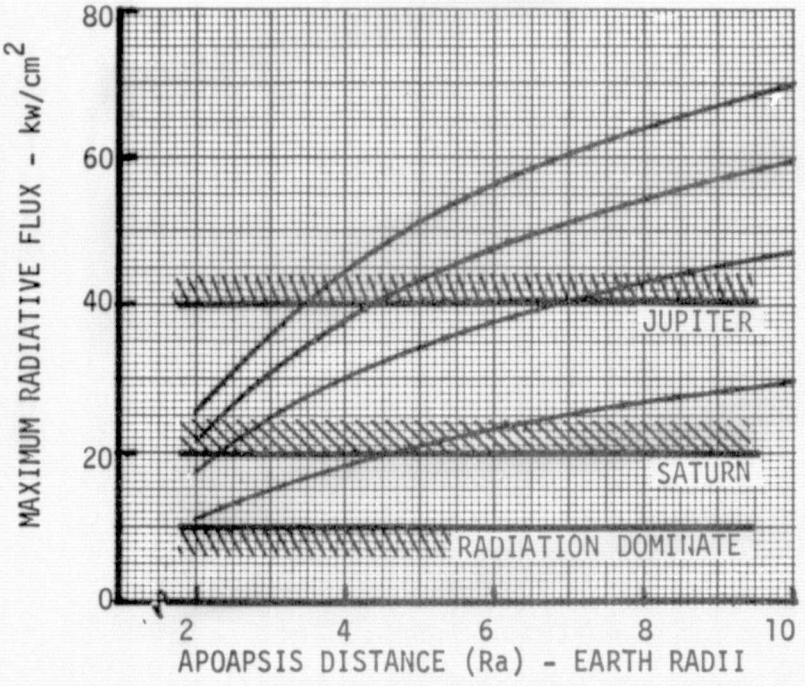

PAYLOAD MASS (kg)	β (kg /m²) *
200	240
150	180
100	120
50	60

*C_DA = CONSTANT

(b) PAYLOAD MASS EFFECT

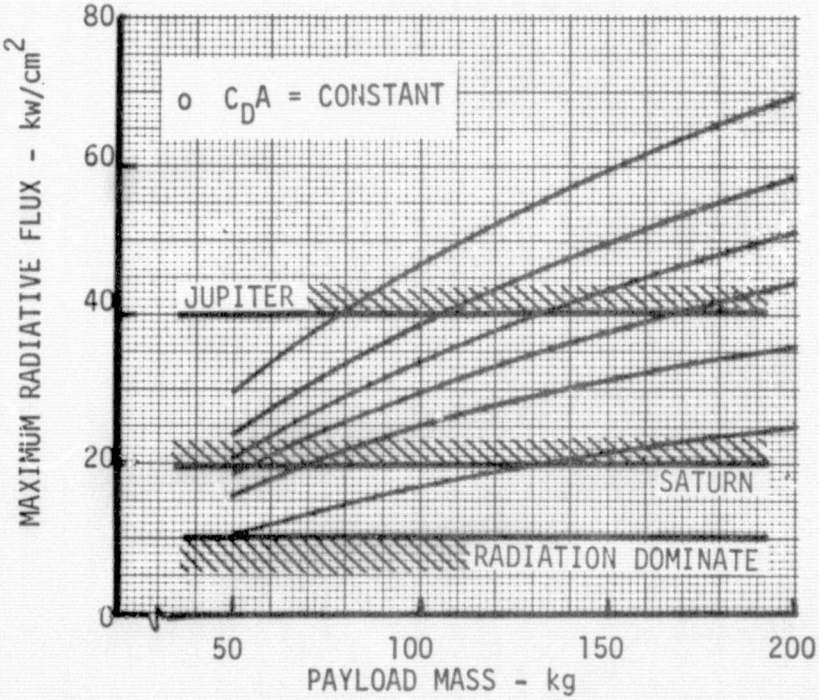

R_a
10
6.6 (SYNC. ALT.)
5
4
3
2

FIGURE 10

EARTH ENTRY SIMULATION CAPABILITY

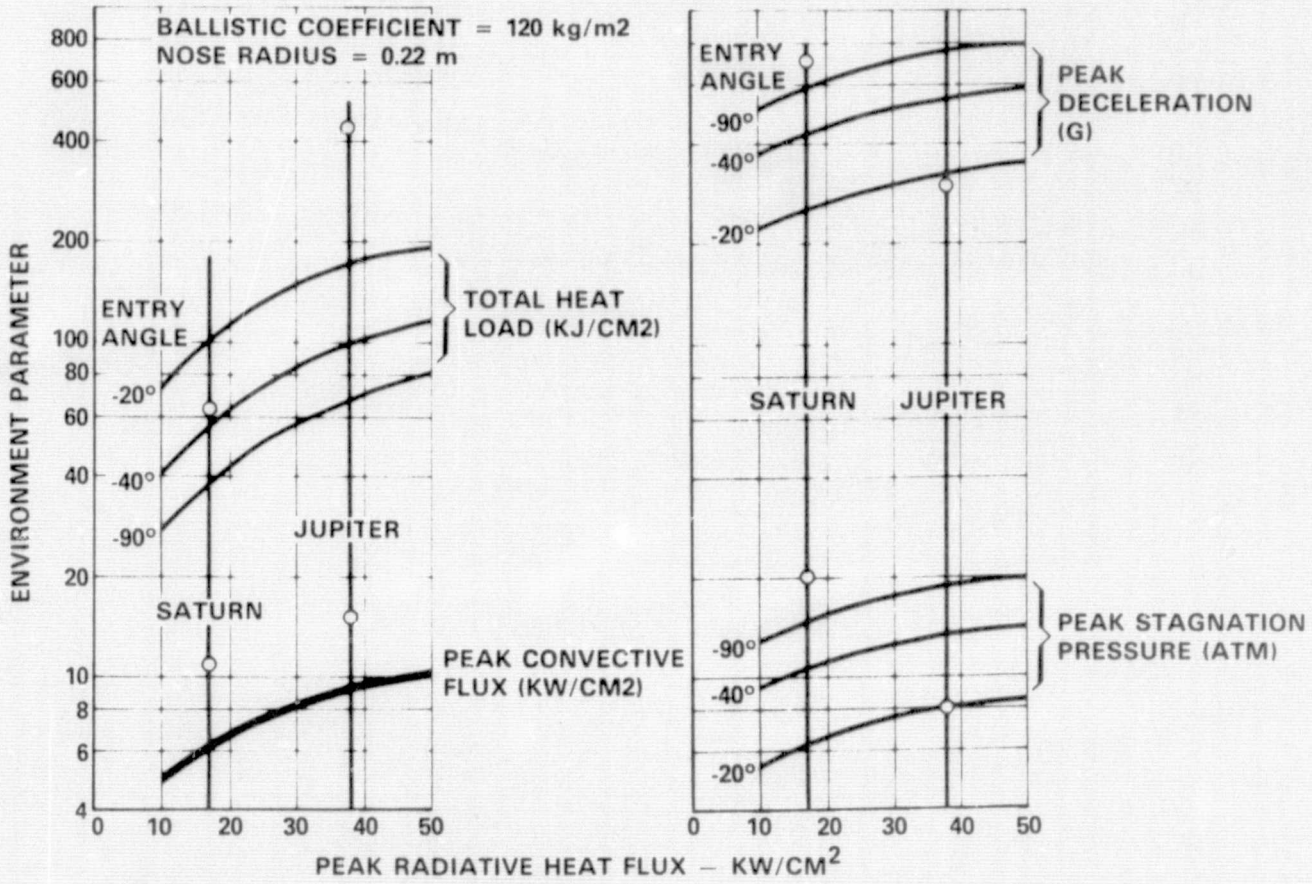

FIGURE 11

match the total heat load for Saturn. However, even the shallowest earth entry falls short of the total heat load for Jupiter. Although this might be of some concern if the flight test is meant to qualify a Jupiter heat shield, it is not expected to be a serious deficiency when the flight test is intended to enlarge the technology base. G-loads and stagnation pressure are closely related and can be nearly matched for either Jupiter or Saturn. The best overall match can be obtained for Jupiter at a 20 degree entry angle. Referring back to Figure 6, it is seen that this requires an earth entry velocity on the order of 20 km/sec. This will of course be extremely difficult to achieve with any but the most energetic upper stage boosters.

Vehicle configuration can also influence the relative as well as the absolute level of environment parameter simulation. In addition to varying the entry velocity and flight path angle, the level of radiation flux can be altered by selecting different ballistic coefficients and different nose radii for the entry vehicle. This is illustrated in Figures 12 and 13. For example, doubling the ballistic coefficient more than doubles raditive flux but increases convective flux by less than 50 percent. Similarly reducing nose radius by a factor of 2 reduces radiative flux by about 20 percent but increases convective flux by approximately 40 percent. This points out the potential use of vehicle configuration "tailoring" as a means of closer simultaneous simulation of environment parameters.

Atmospheric Composition Causes Shift in Spectral Flux - The atmosphere composition differences raise the issue of shock layer radiation spectral distribution. The incident radiation sepctrum is a complex function of many variables, chief among which are gas composition, total energy, density and shock layer thickness. The shock layer radiation interacts with the boundary layer gases so that the spectral intensity and total radiant energy incident on the heat shield surface can differ significantly from the initial shock layer values. While planetary entry levels of radiative heating can be simulated during earth entry, the difference in atmosphere composition results in a different spectral distribution. Air shock layers radiate nearly 50 percent of their intensity in the vacuum ultra violet (VUV), whereas most of the radiation in hydrogen-helium mixtures occurs in the ultra violet, visible and infrared regimes. Typical spectral distributions for Jupiter and earth entries are shown in Figure 14.

There are obviously similarities as well as differences. Both have qualitatively similar distributions. The Jupiter distribution peaks in the visible spectrum and

EARTH ENTRY ENVIRONMENT SENSITIVITY TO BALLISTIC COEFFICIENT

- o STAGNATION POINT
- o NON BLOWING
- o β_{REF} = 120 kg/m^2
- o $(R_N)_{REF}$ = .22 m

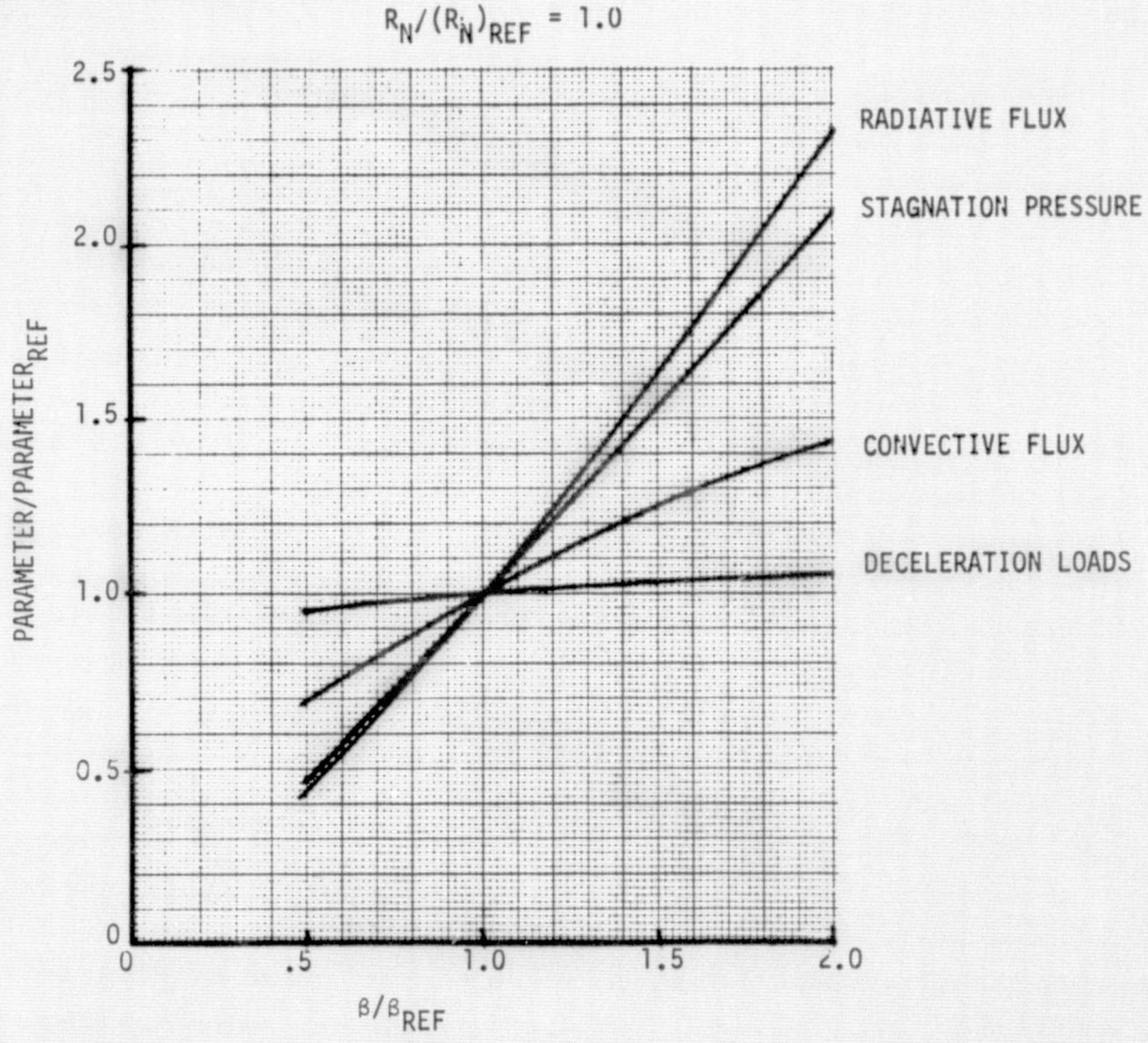

FIGURE 12

EARTH ENTRY ENVIRONMENT SENSITIVITY TO NOSE RADIUS

- o STAGNATION POINT
- o NON BLOWING

$\beta_{REF} = 120\ kg/m^2$

$(R_N)_{REF} = .22\ m$

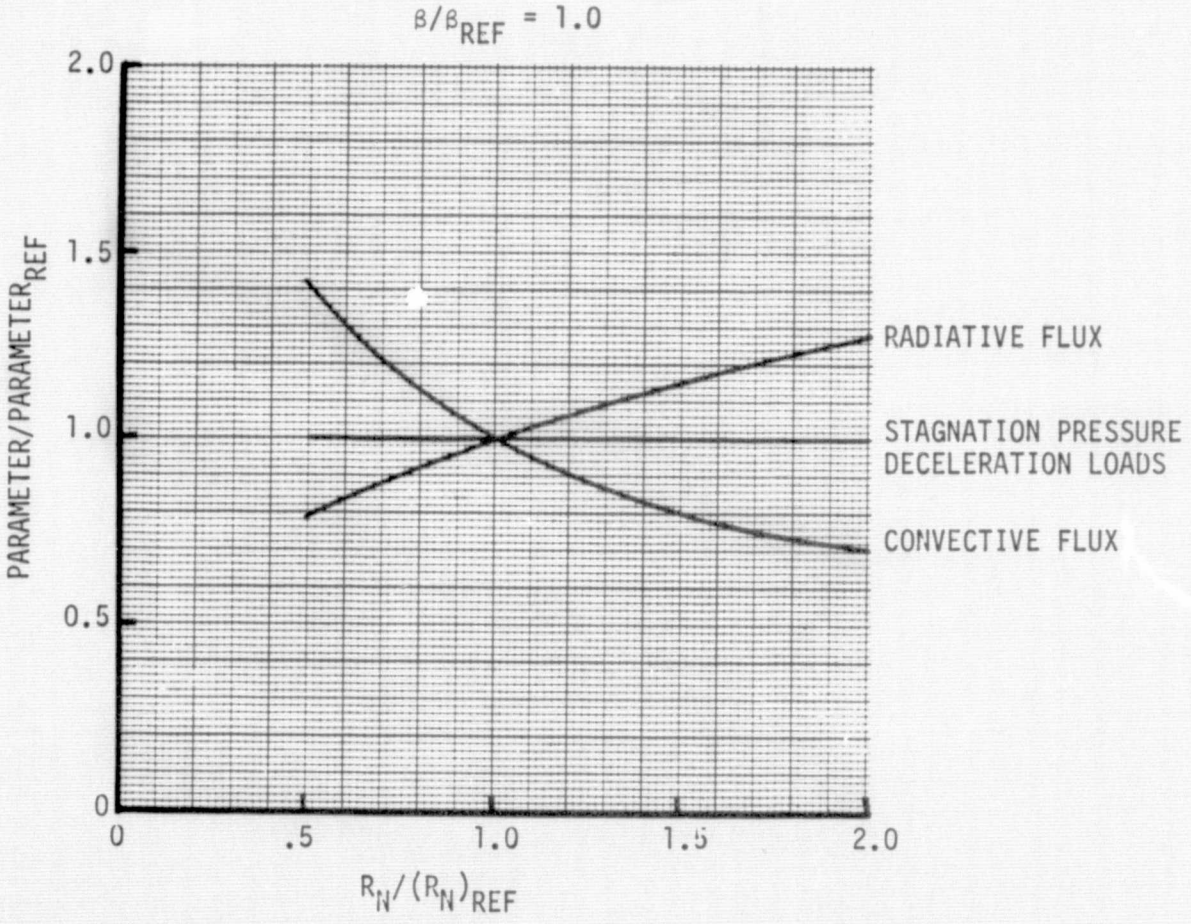

FIGURE 13

SPECTRAL DISTRIBUTION CONSIDERATIONS

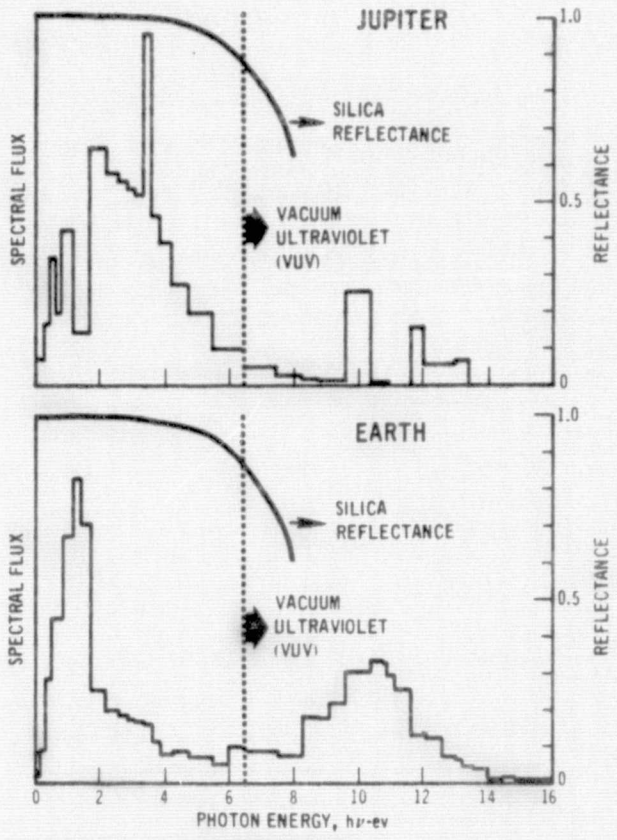

ENERGY DISTRIBUTION*	PLANET	
	JUPITER	EARTH
% BELOW VUV	80	50
% ABOVE VUV	20	50
% ABSORBED (SILICA)	26	50

*PEAK RADIATIVE FLUX
STAGNATION POINT
NON-BLOWING

FIGURE 14

again in the VUV at about 11 electron volts. The earth distribution peaks in the near-infrared and also in the VUV at 10-11 electron volts.

While the spectral distribution differences are of little concern for testing carbonaceous heat shields, they are a consideration in testing reflective silica heat shields. Since the reflectivity of silica is spectrally dependent as depicted in Figure 14, only about half of the incident radiation from an air shock layer will be reflected. This is not expected to destroy the validity of such a test. Indeed if the silica heat shield can absorb the higher energy radiation in addition to the convective heating, it will demonstrate the effectiveness of a reflective heat shield in an environment even more severe than it was intended to experience. Another consideration is the possible blocking of the VUV radiation by the ablation products of the silica heat shield for either earth or Jupiter entries. In any event, the correlation of predictive techniques with flight test results will provide a basis for increased confidence in the design of planetary probe heat shields.

Blowing Radiative Flux can be Simulated - The intense radiative flux emanating from the shock layer is significantly reduced due to mass injection and cooling effects caused by heat shield ablation. Detailed studies using shock layer flow field/radiation computer codes showed the effect of shock layer temperature distribution, wall temperature, standoff distance and species concentration on the incident heating. Detailed analyses were made for several Jovian and Earth flight conditions, and for three heat shield materials; carbon, carbon phenolic and hyperpure silica. Figure 15 shows a comparison of typical Jovian heating conditions with peak flux during earth entry from V_E = 16.76 km/sec as a function of entry angle. Both the incident and net radiative fluxes to a carbon shield can be matched by entering at a steeper angle, -22 degrees. The incident flux on the silica shield is matched at -48 degrees but the net flux will be substantially greater than predicted for Jupiter. This increase is beneficial because the total heat absorbed by the heat shield will more closely simulate that predicted for Jovian entry.

Due to uncertainties in Jovian entry conditions, the maximum design radiative heating is slightly higher than the predicted for a typical entry. The capabilities to simulate the corresponding radiative heating, considering blowing effects, using the Transtage/TE364-4 and the SRM IUS/TE364-4 are shown in Figure 16. The required incident heat to both the silica and the carbon phenolic shields can be simulated using the Transtage. Apoapsis of about 12 earth radii are required for the silica and 14 for the carbon phenolic. The next flux can be matched for the carbon phenolic but the net flux to the silica will be substantially greater than the Jovian entry.

HEAT SHIELD RADIATION PERFORMANCE FOR EARTH ENTRY

(BASED ON JOVIAN SIMILAR SHOCK PROFILES)

V_E = 16.76 KM/SEC

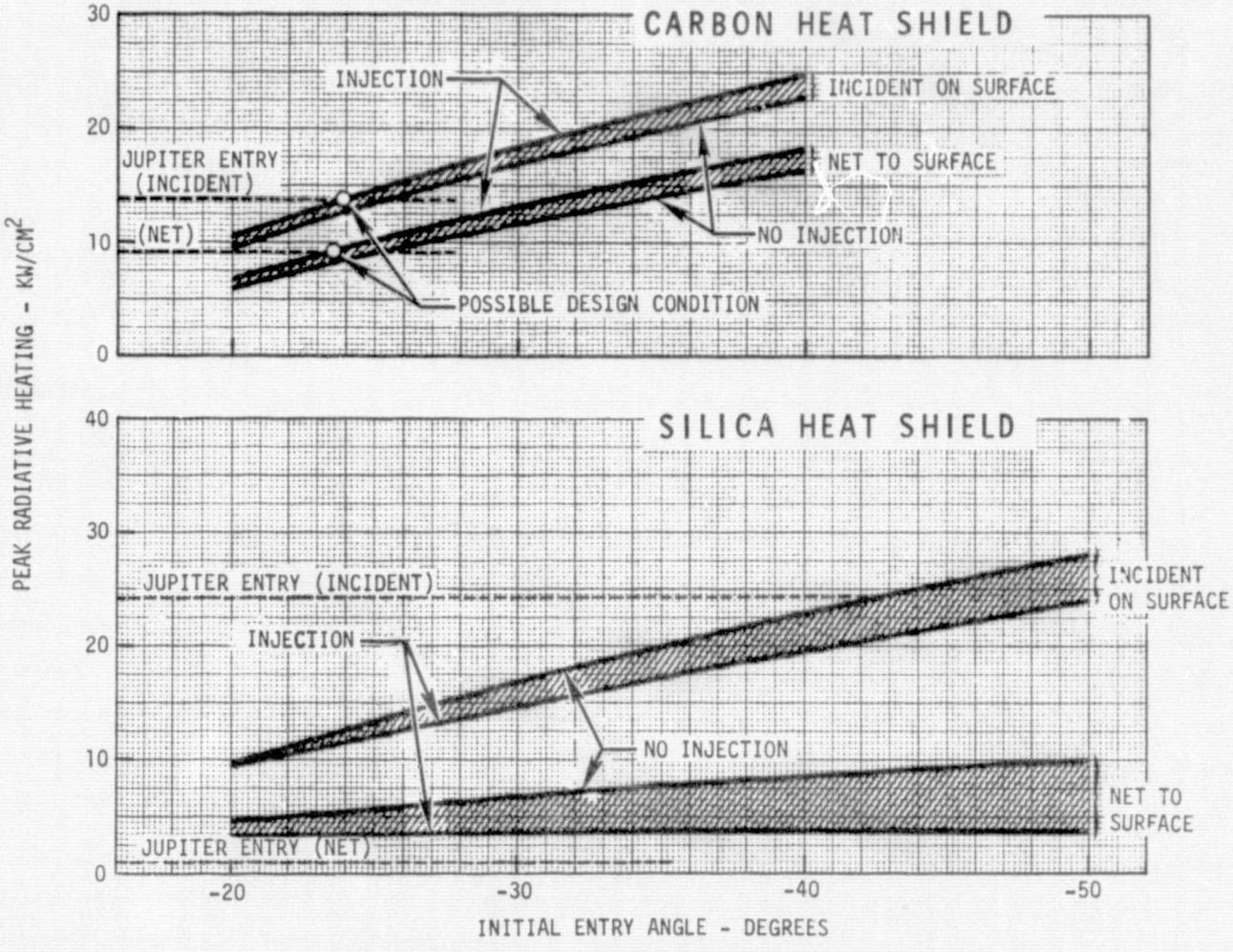

FIGURE 15

BLOWING RADIATIVE FLUX SIMULATION – EARTH

(100 kg; β = 100 kg/m^2 VEHICLE)

TRANSTAGE/TE364-4

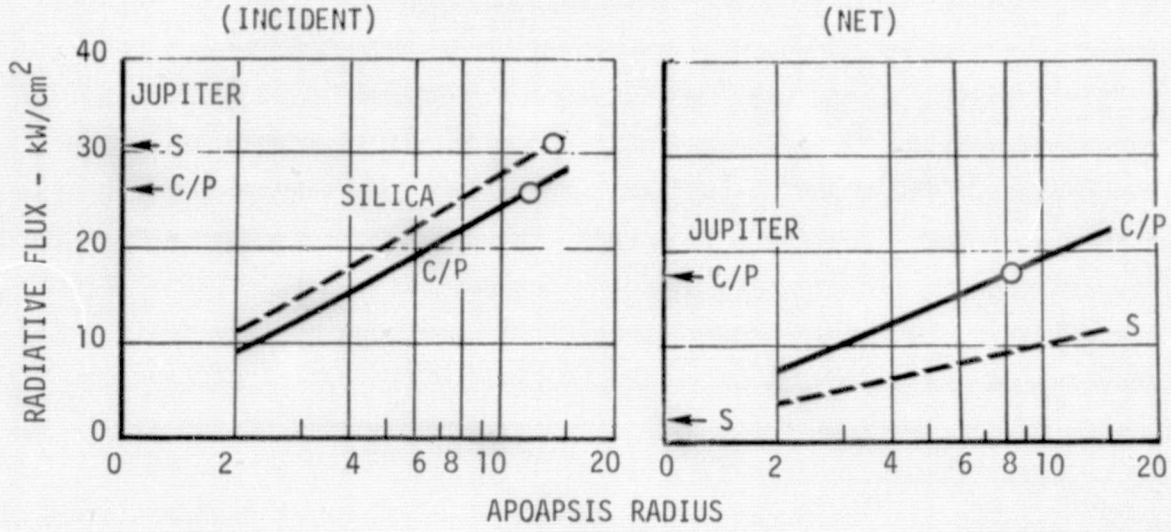

SRM IUS/TE364-4

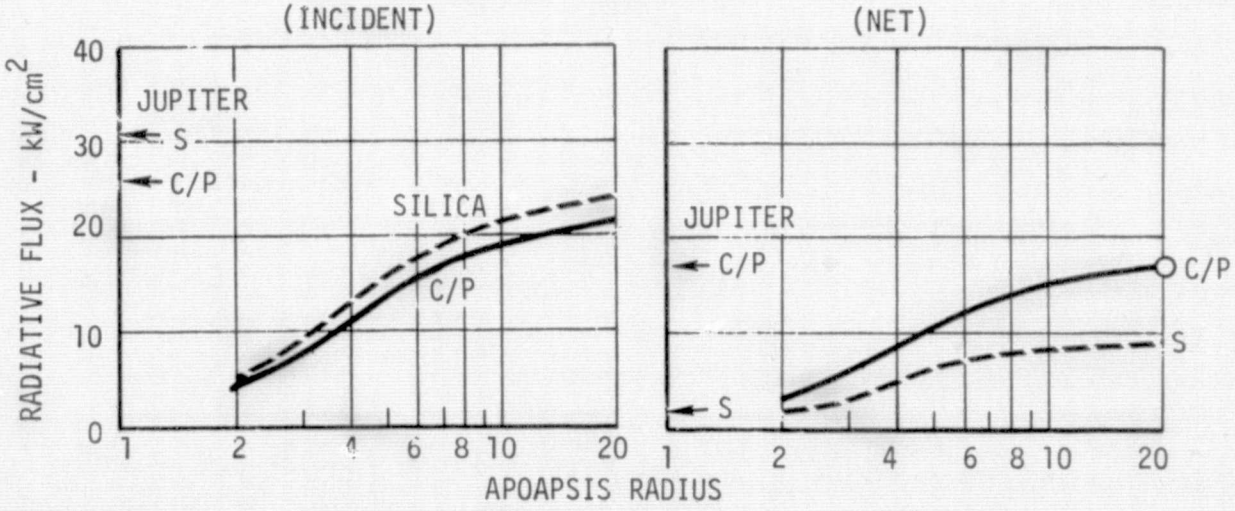

C/P - CARBON PHENOLIC
S - SILICA

FIGURE 16

The net flux to the silica shield can be simulated using either the Transtage or IUS by flying low apoapsis trajectories. Using the IUS to simulate carbon phenolic shield net flux is possible by flying to R_a = 20 but the incident flux falls short of the required 26.6 kW/cm^2. Similarly an IUS boost does not produce the desired incident flux (30.5 kW/cm^2) on the silica shield. However, very high radiative fluxes are possible and obtaining data in this radiation dominated regime, even with some mis-match, is worthwhile and will increase the technology base.

Radiometer Design is the Only Instrumentation Area Requiring Development - The instrumentation needs of the entry vehicle can be met with standard, commercially available equipment. The anticipated high acceleration may require more rugged packaging than is usually required. The only item which will require some development is the radiometer. In order to keep the package size small, optical focal lengths must be short, which in turn requires that detectors be physically small so that they can be spaced consistent with the small differential diffraction angles. Previous space probes, such as the Skylab ATM experiments, used photomultiplier tubes as detectors. These are too large for this application.

A major problem in radiometer design is the measurement of vacuum ultraviolet energy, particularly in the range below 0.25 microns. Traditional window materials such as fuzed quartz are opaque in this region. The only known material which will pass radiation down to 0.12 microns is lithium fluoride. However, this material is thermally and mechanically inferior to quartz and therefore will require environmental protection. The designs shown in Figures 17 and 18 consist of an open port through the heat shield and the window located at the entrance to the radiometer. Helium flow past the window provides cooling and a purge pressure that reduces the possibility of heat shield fragments clogging the port. In the multichannel design shown in Figure 17, the helium tank is external to the radiometer package. The spectral scanning design of Figure 18 shows a helium tank and electrically operated shut-off valve inside the package.

Comparing the two designs, the multichannel radiometer has the advantage of simplicity, since there are no moving parts and the construction can be sufficiently rigid that the optical characteristics are not affected by the flight environment. The amplitude of the signals seen by the detectors in the twelve channel design are time variant only, within the spectral bandwidth of the filters used; whereas in the spectral scanning design, the signal is both time and wavelength variant as a function of the rotating mirrors which scan the gratings. The use of many discrete channels has the advantage of design simplicity but enough channels must be

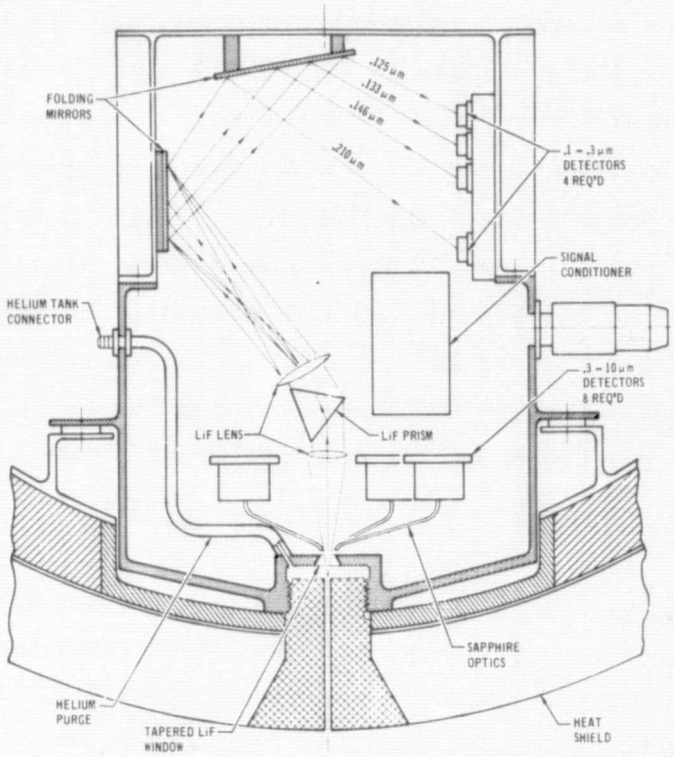

MULTICHANNEL RADIOMETER

FIGURE 17

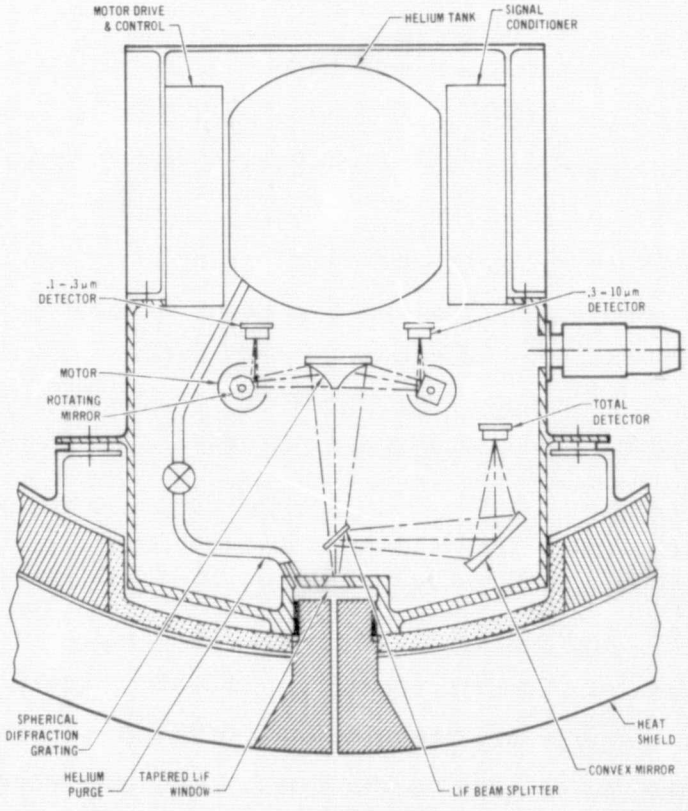

SPECTRAL SCANNING RADIOMETER

FIGURE 18

available to adequately define the spectral energy distribution. The maximum number of channels is limited by space available in the vehicle for the radiometer package. Use of two scanned channels (one for UV from 0.1 to 0.3 microns and one for visible and IR from 0.3 to 10 microns) provides better spectral coverage but the need for motors to drive the mirrors makes the radiometer design more complex. Calibration and subsequent data processing are also made more difficult since the mirror position must be measured and correlated with the radiometer data to avoid spectral wavelength errors. The motor speed must be constant and unaffected by in-flight environmental conditions. A prism and lens was shown in one design and a diffraction grating in the other. Either diffraction device will work in either design. More detailed design, including cost estimates, will be required to determine the best choice.

A Recoverable, Probe Shaped Entry Vehicle Design is Feasible - An earth entry test vehicle design was derived by modifying the results of previous outer planet probe studies to include a mid-air recovery system and to reflect differences in mission test objectives. The resulting configuration illustrated in Figure 19 is a blunted 60-degree half angle cone with a hemispherical afterbody and a maximum diameter of 89 cm. The primary structure of the forebody consists of an aluminum ring-stiffened conical shell bonded to phenolic honeycomb. The internal rings provide both shell stiffening and provisions for mounting internal subsystem equipment. The afterbody is a fiberglass honeycomb structure covered with a thin layer of RF transparent elastomer for heat protection. Subsystem equipment are listed on Figure 19. A typical recovery sequence is shown in Figure 20.

A detailed mass property analysis indicated that ballasting for stability actually enhanced radiative flux simulation capability and also offered a simplified structural design option. Two interrelated aspects were considered: (1) the amount of ballast needed to provide a proper entry center of gravity (c.g.) location and (2) the increase in ballistic coefficient (β) attainable by increasing only vehicle mass.

The concern for c.g. location arises from the requirement for a positive static stability margin. Hence the longitudinal c.g. location must be prevented from being appreciably aft of the theoretical cone/hemisphere intersection plane. The location of this aerodynamic reference plane is shown in Figure 21. However, equipment arrangement, particularly the necessarily aft location of the recovery parachute system, indicated the probable need to ballast in the forward, conical section.

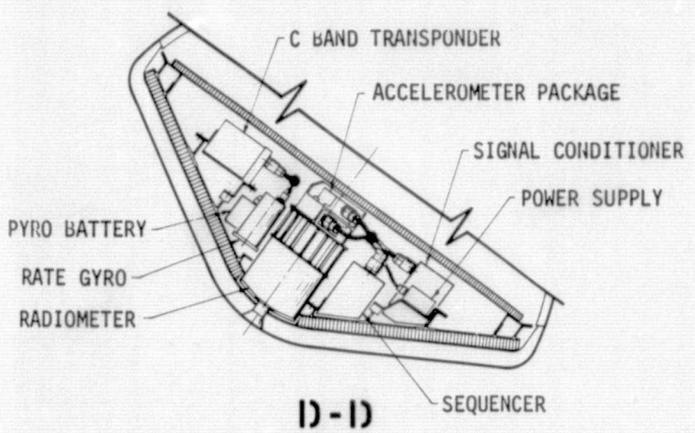

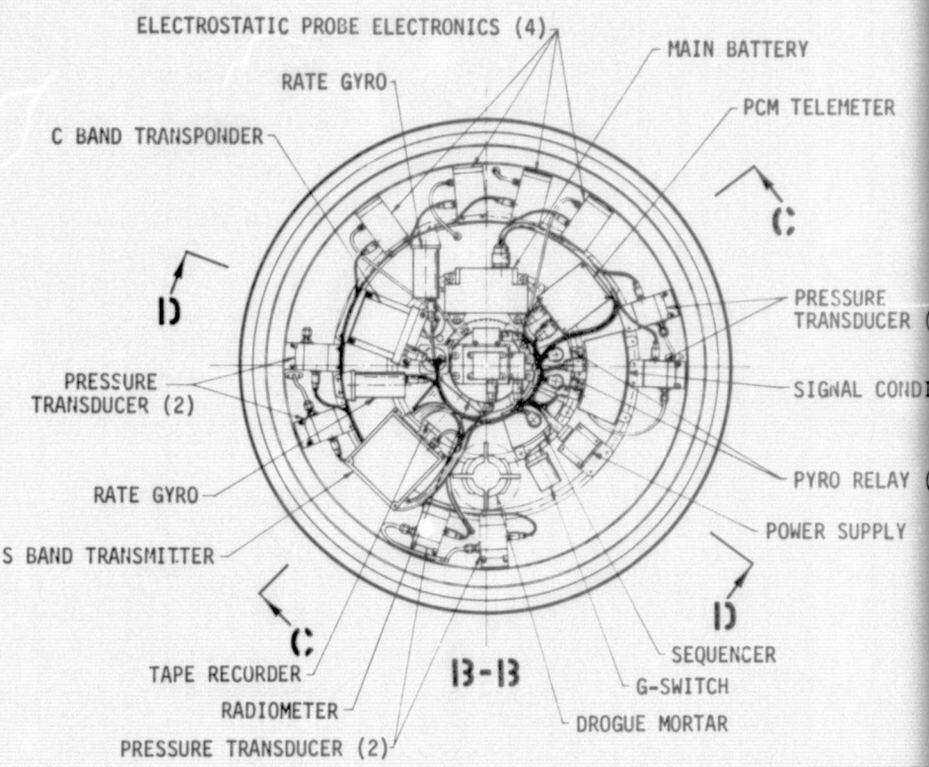

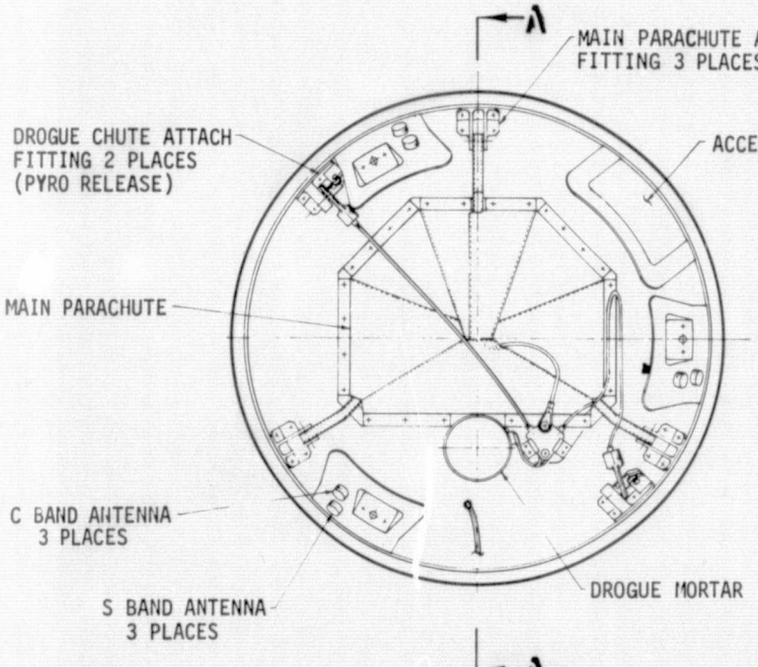

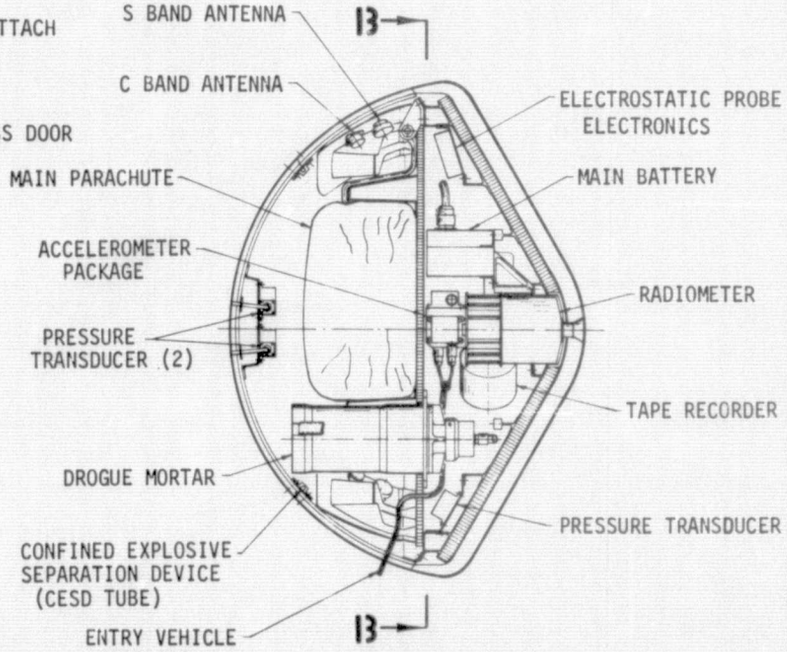

TYPE
SEQUENCER
MAIN BATTE
RADIOMETER
ELECTROSTA
PROBE ELEC
ACCELEROM
RATE GYROS
PRESSURE T
STRAIN GAG
THERMOCOUP
(PLUGS)
SIGNAL CON
POWER SUPP
PCM TELEME
TAPE RECOR
S-BAND TRA
S-BAND ANT
C-BAND BEA
TRANSPON
C-BAND ANT
PYRO BATTE
PYRO RELAY
CONF. EXPL
DEV.
G-SWITCH
DROGUE MOR
DROGUE PAR
MAIN PARAC

EARTH ENTRY VEHICLE
INBOARD PROFILES

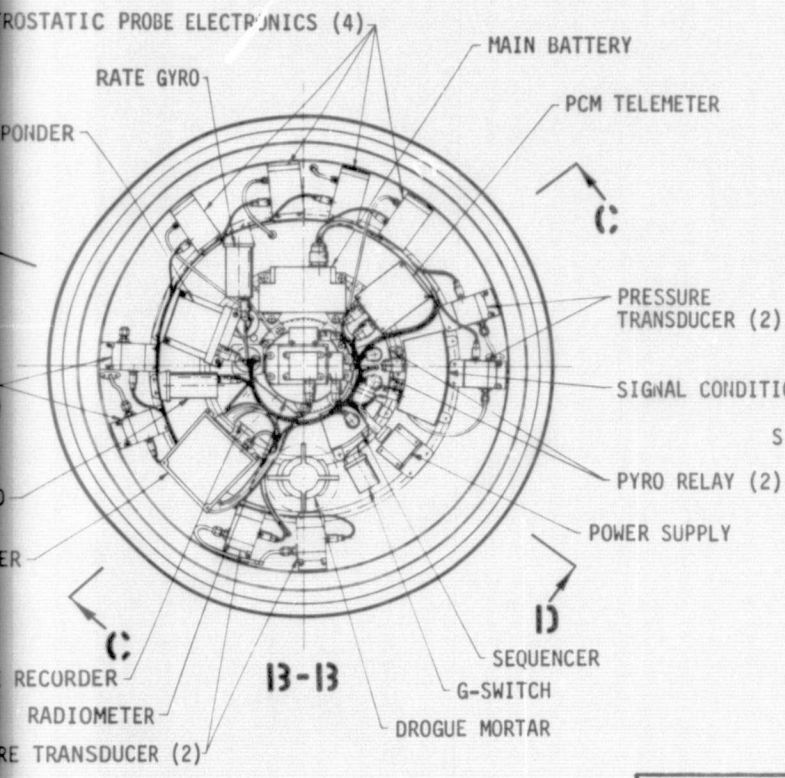

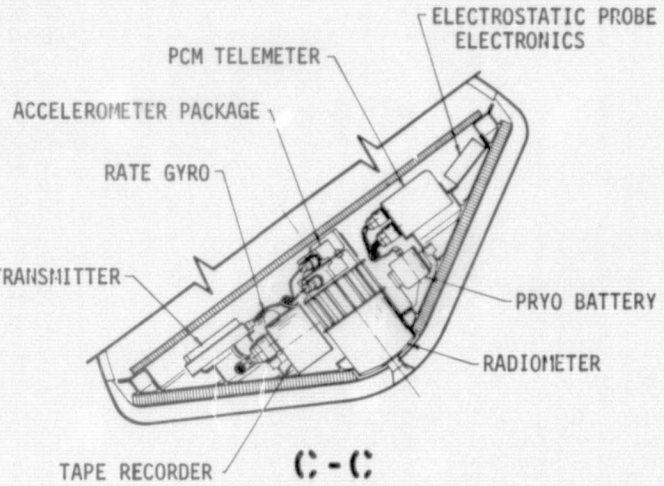

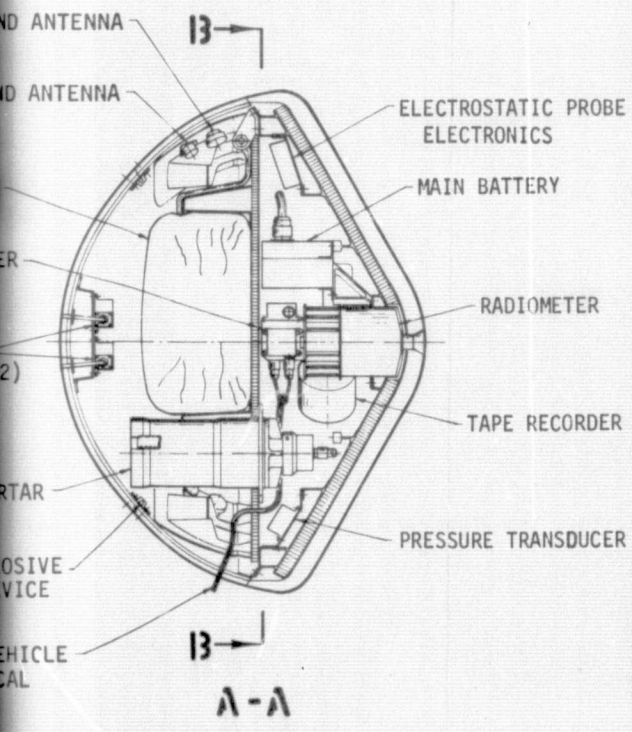

EQUIPMENT LIST

TYPE	FUNCTION	ACTIVE MISSION PHASE				
		PRE-SEP.	PROBE SEP.	PRE-ENTRY	ENTRY	RECOVERY
SEQUENCER	CONTROLS SEPARATION & RECOVERY EVENTS	X	X			X
MAIN BATTERY	ELECTRICAL POWER FOR ALL EQUIP. EXCEPT PYROS		X	X	X	X
RADIOMETER	ATMOSPHERIC DATA			X	X	
ELECTROSTATIC PROBE	ATMOSPHERIC DATA			X	X	
PROBE ELECTRONICS	PROBE POWER & SIGNAL COND.			X	X	
ACCELEROMETER PKG.	3 AXIS VEHICLE MOTION DATA			X	X	
RATE GYROS	3 AXIS VEHICLE MOTION DATA			X	X	
PRESSURE TRANSDUCERS	SURFACE PRESSURE DATA			X	X	
STRAIN GAGES	STRUCTURAL DEFLECTION			X	X	
THERMOCOUPLES (PLUGS)	HEAT SHIELD TEMPERATURE & ABLATION			X	X	
SIGNAL CONDITIONER	DATA SENSOR SIGNAL MODIFICATION			X	X	
POWER SUPPLY	DATA SENSOR POWER			X	X	
PCM TELEMETER	DATA MULTIPLEXER & DIGITIZER			X	X	
TAPE RECORDER	RECORD ENTRY DATA				X	X
S-BAND TRANSMITTER	PCM DATA TRANSMITTER			X	X	X
S-BAND ANTENNAS	RADIATE PCM SIGNAL			X	X	X
C-BAND BEACON TRANSPONDER	RECEIVE & RETRANSMIT TRACKING SIGNAL				X	X
C-BAND ANTENNAS	RECEIVE & RADIATE TRACKING SIGNAL				X	X
PYRO BATTERY	EXPLOSIVE DEVICE POWER					X
PYRO RELAY	TRIGGERS DROGUE MORTAR & CESD					X
CONF. EXPLO. SEP. DEV.	SEPARATES AFT BODY COVER					X
G-SWITCH	INITIATES RECOVERY SEQUENCE					X
DROGUE MORTAR	DEPLOYS DROGUE PARACHUTE					X
DROGUE PARACHUTE	DEPLOYS MAIN PARACHUTE					X
MAIN PARACHUTE	VEHICLE RECOVERY					X

FIGURE 19

FOLDOUT 2

RECOVERY SEQUENCE

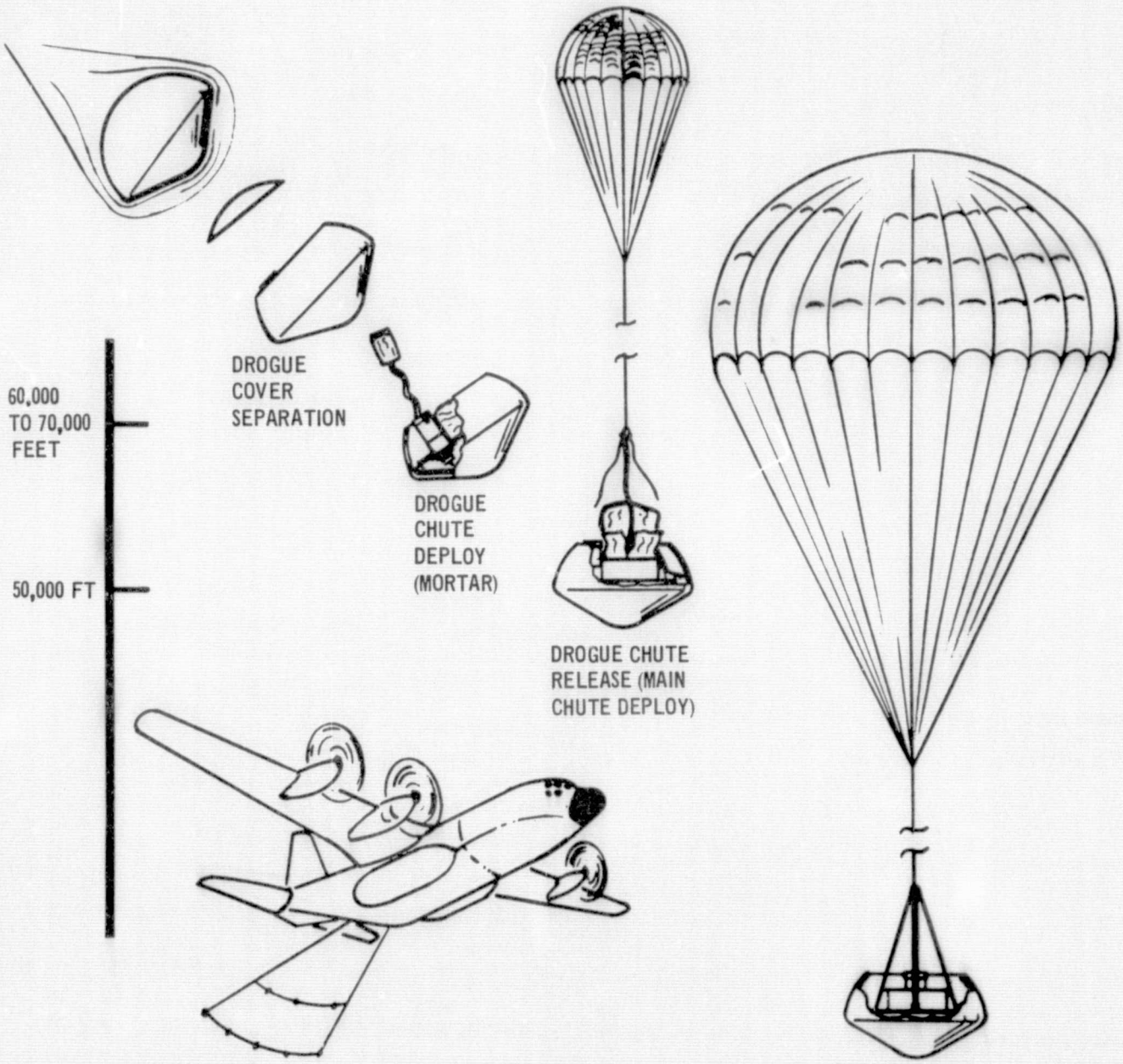

FIGURE 20

BALLAST LOCATION

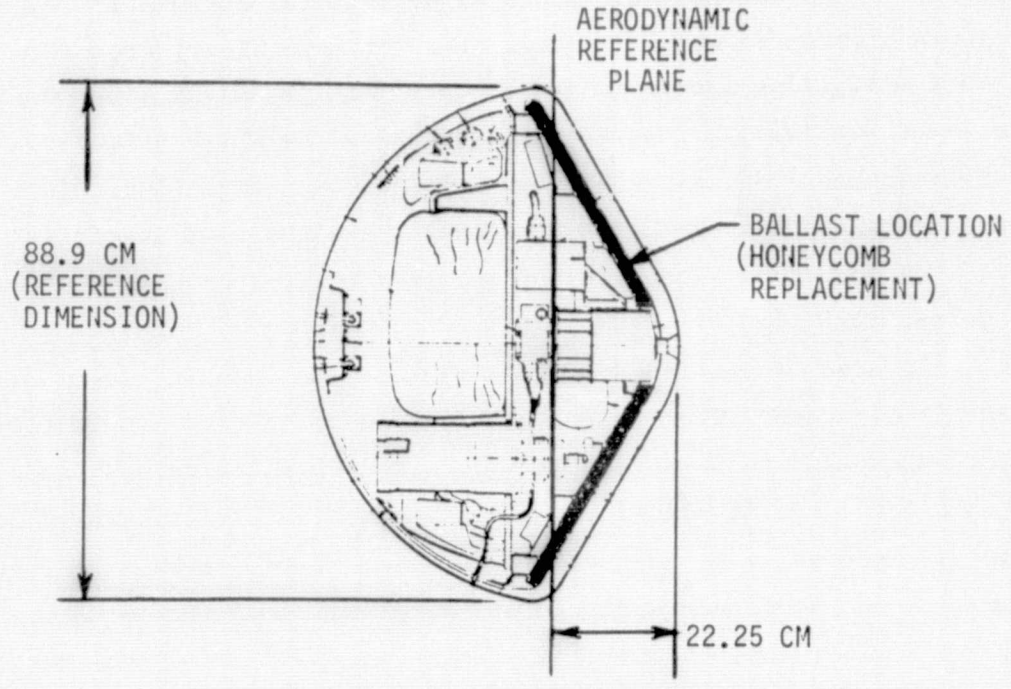

FIGURE 21

LONGITUDIANL BALLAST SUMMARY

	BALLAST CRITERIA		
	NONE	MINIMUM	MAXIMUM
BALLAST MASS (kg)	0	21.90	107.99
VEHICLE C.G. LOCATION FROM NOSE (cm)	24.73	22.25	21.25
FROM REF. PLANE (% OF REF DIMENSION)	2.7 (AFT)	0	1.2 (FWD)
TOTAL VEHICLE MASS (kg)	109.42	130.94	215.42
BALLASTIC COEFFICIENT (kg/m^2)	113.92	136.32	224.27

FIGURE 22

Further, a significant amount of ballast was anticipated because of the blunt body shape which offers a relatively short ballast moment arm.

Ordinarily, a large ballast mass would be detrimental because it reduces the ΔV available from a given booster. However, the corresponding increase in ballistic coefficient is a mitigating factor unique to this high radiative flux simulation mission. As noted previously, increasing β decreases the entry velocity and hence the booster ΔV required to simulate a given level of radiative flux. If β is increased only by mass addition ($C_D A$ = constant) the net effect is still advantageous. The reduction in booster ΔV required is greater than the reduction in booster ΔV capability.

Entry vehicle mass properties were determined using computer codes developed for the outer planet probe. The effect of ballast mass on total vehicle mass, ballistic coefficient and center of gravity locations was determined. Representative results are tabulated in Figure 22 and are graphically illustrated in Figure 23. Ballast was assumed to be in the form of steel plate segments that replace the honeycomb core of the forward heat shield structure (ref Figure 19). As expected the "no ballast" case resulted in a c.g. location aft of the aerodynamic reference plan. However, it was only displaced by .98 cm (2.7% of reference dimension) relative to the reference plane which was not as far aft as anticipated. While this is marginally acceptable, a c.g. location at or forward of the aerodynamic reference plane was considered necessary at this preliminary design stage to insure an adequate stability margin in the final configuration. Hence a minimum ballast case was investigated in which just enough aluminum honeycomb core was replaced with steel plate to move the c.g. forward to the aerodynamic reference plane. This 21.9 kg of ballast increased total vehicle mass from about 109 kg to 131 kg and β from approximately 114 kg/m^2 to 136 kg/m^2. Although this provided a satisfactory c.g. location it did not represent a maximum ballistic coefficient configuration. A maximum ballast case was therefore evaluated in which all of the aluminum honeycomb core was replaced with steel plate. The resulting 108 kg of ballast increased vehicle mass to 215 kg and β to 224 kg/m^2, while moving the c.g. forward of the reference plane by 1.2% of reference dimension. Since this is substantially higher than the 120 kg/m^2 value assumed for the earth entry environment analysis, a net reduction in required booster performance is possible. Further, the maximum ballast case offers a unique vehicle design opportunity. A simple, steel structural shell can be used rather than the more sophisticated honeycomb

LONGITUDINAL BALLAST EFFECTS

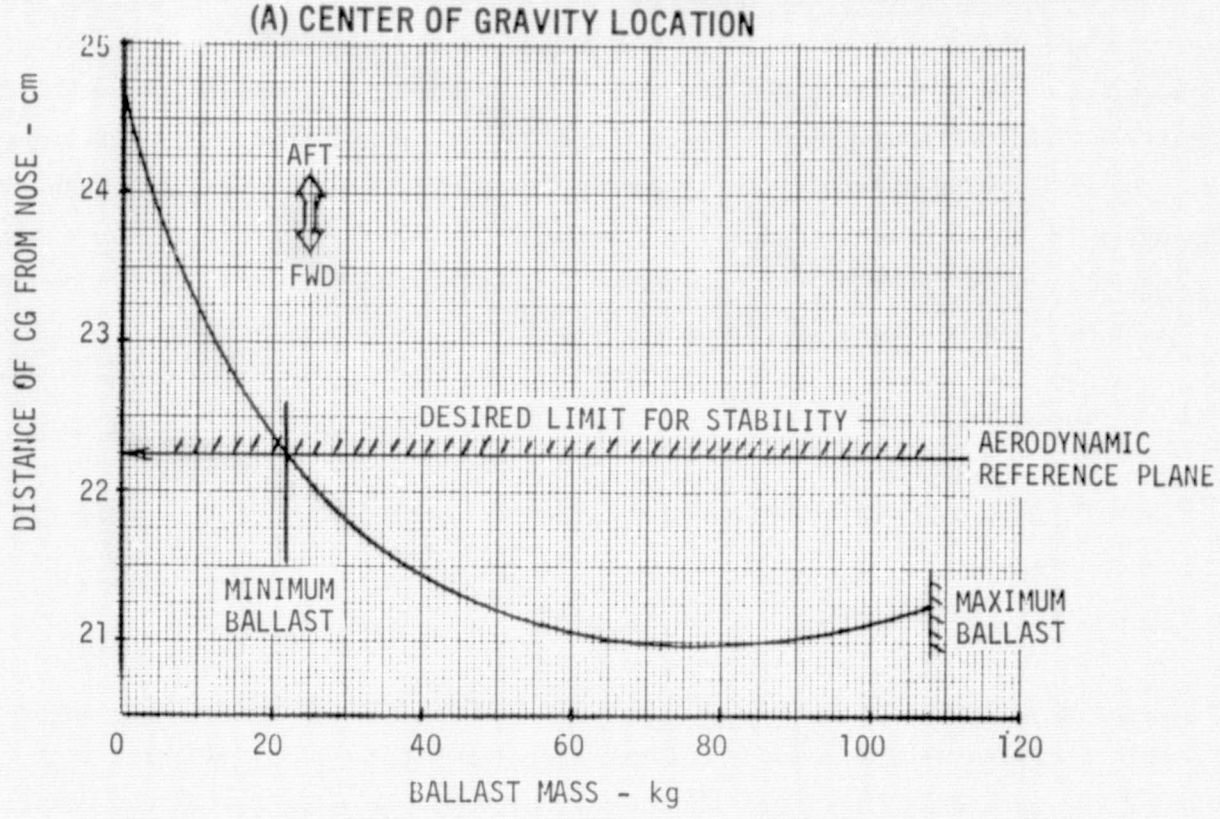

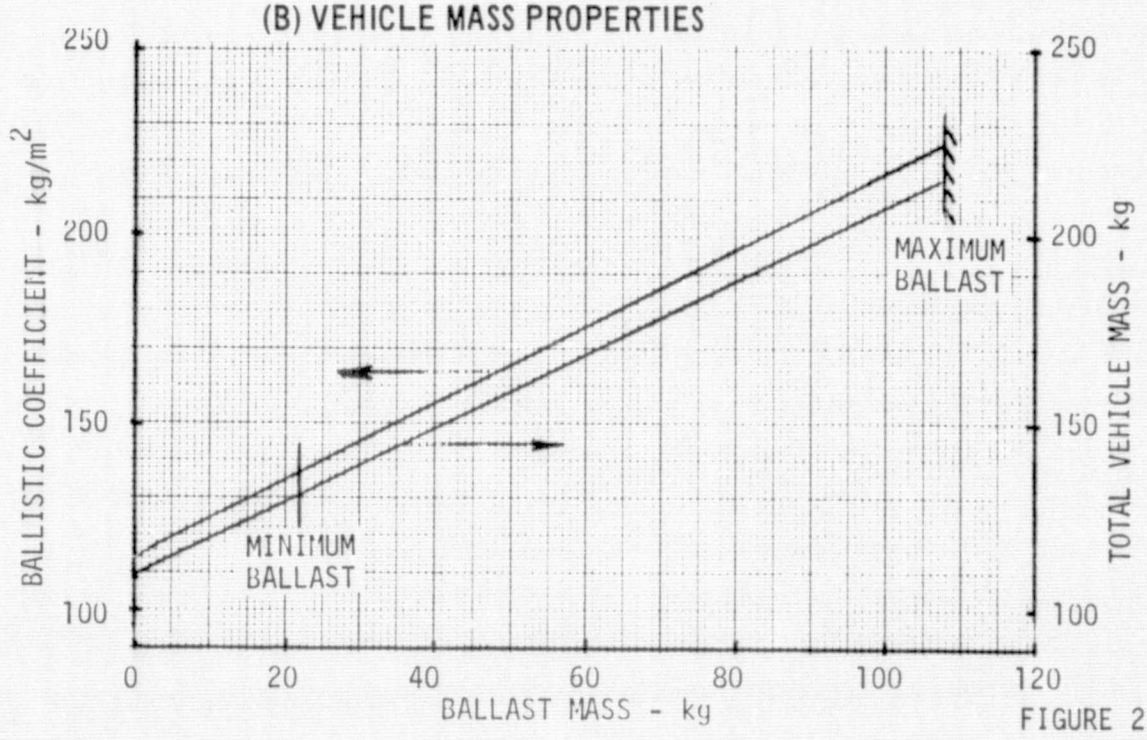

FIGURE 23

structure. This would provide a less expensive structural design that also minimizes booster performance requirements and insures a proper c.g. location.

Total Recurring Cost Per Flight is Estimated to be 11\overline{M}$ - The cost of conducting an earth entry flight consists of expenses chargeable for a Shuttle launch, the booster, the entry vehicle, its recovery and the reduction of data. Rough-order-of-magnitude (ROM) estimate show a $11.5 $\overline{M}$ non-recurring and a $3.2 $\overline{M}$ recurring costs for designing, fabricating, testing and delivery of the entry vehicle. Sharing the expense with other cargo reduces the projected Shuttle launch cost. The total recurring cost per flight, including Shuttle, booster and recovery services were examined to determine possible cost spread.

Type of Launch	Dedicated	Shared
Shuttle	$12.0 $\overline{M}$	$7.0 $\overline{M}$
Booster	1.0	
Entry Vehicle	3.2	3.2
Recovery	.3	.3
Data Reduction	.5	.5
	$17.0 $\overline{M}$	$11.0 $\overline{M}$

Dedicated Shuttle launch cost of $12 $\overline{M}$ (1976 dollars) was obtained by escalating the 1974 estimate of $10.3 $\overline{M}$. If either Transtage/TE364-4 or the solid rocket motor IUS/TE364-4 were used less than 3/8 of the bay would be used and if the "short length" booster were used only 1/7 would be occupied. Launch cost should be reduced accordingly. The booster cost of $1.0 $\overline{M}$ is the current figure being quoted for the solid IUS in the open literature. Costs of the other boosters considered range from $3 $\overline{M}$ to over $6 $\overline{M}$. The shared launch cost of $7.0 $\overline{M}$ for Shuttle and booster reflects either a solid IUS with 50% payload sharing or a short length booster that occupies the space of one pallet.

Now is the Time to Move Forward with Vehicle Design and Mission Planning - Recommendations for additional studies, instrumentation development and heat shield testing have been identified in this study. Six areas requiring more detailed study are radiative heating during Jovian entry, radiative during earth entry, the effects of heat shield ablation species on the radiative heating, effects of mass injection on convective heating, modeling of ablator energy balance/surface recession and the thermochemical structural capabilities of candidate heat shields.

The capabilities and limitations of the radiometer candidates for the entry vehicle should be analyzed and verified by testing. Measuring radiative flux intensities in the vacuum ultra violet is important because a significant portion of the

incident energy is contained in this regime. Arc tunnel testing of candidate heat shield materials is needed to better understand material behavior and to correlate measured performance with predictions. It is further recommended that the radiometers be used to measure the radiative environment during the testing of ablators, thereby making in situ measurements and qualifying hardware.

By accomplishing an earth entry experiment, design conservatism for a successful outer planet mission will be decreased. This, in turn, can make more mass available for experiments. The next phase of vehicle design should include design, fabrication and testing of an engineering model to establish reliability. As part of the mission planning, the entry experiment needs to be factored into the Shuttle traffic model and a range safety/dispersion analysis conducted.

Accomplishment of these tasks will vastly expand the technology for the exploration of the solar system.

DOD ENTRY TECHNOLOGY FLIGHT EXPERIMENTS

DOD ENTRY TECHNOLOGY FLIGHT EXPERIMENTS

The Space Shuttle can provide unique simulation capability for DoD reentry vehicle experiments. The areas of uniqueness are listed in Figure 24. They emphasize the fact that the Shuttle is a mobile launch platform, is at earth orbital velocity, has a high weight payload capability, and can provide payload overflight at many desirable impact areas. The principal study conclusions are summarized below:

Shuttle will be of Benefit in Meeting DoD Needs in the 1980's - The identification of DoD reentry vehicle test needs for the 1980's was accomplished through interface meetings with SAMSO/Aerospace and subsequent documentation. Such testing will continue to have high priority as the state of the art expands in nose tip technology, heat shields, maneuvering reentry vehicles, terminal guidance, environment survivability provisions, penetration aids, multiple reentry vehicle deployment, and discrimination technology. The Shuttle may be of benefit by providing: (a) unique capability not available in ground launch systems, (b) targeting flexibility for investigating reentry into nontraditional impact areas and adverse atmospheric environments (rain, ice, snow), and (c) conducting numerous experiments with a single launch. For example, the typical, multiple payload DoD mission shown in Figure 25 can be performed by Shuttle launches from either KSC or VAFB into a nominal 160 NMI circular orbit and can provide DoD payload impact at Kwajalein, Poker Flat or Hawaii.

KREMS Radars at KMR Can Track Shuttle Deployed Experiments to Impact - Payload approach corridors at KMR for which KREMS radar coverage to impact is possible are identified in Figure 26. Shuttle deployed payloads can be targeted for the southwest or northwest corridor. As a consequence, data will be of the same type, amount, and quality as that currently acquired from a VAFB to KMR launch into the northeast corridor at KMR. The southwest corridor is achievable from either a KSC or VAFB launch.

Shuttle can Provide Payload Impact at KMR, Poker Flat, and Hawaii - The KMR impact point shown in Figure 27 is south of Kwajalein Atoll and provides KREMS radar aspect angles and slant ranges comparable to those achieved by current ground launches from VAFB. The impact point at Poker Flat, shown in the shaded area of Figure 28,is in a sounding rocket impact zone and provides up to 1000 NMI overland trajectory prior to payload impact. Preferred impact points within tracking range

UNIQUE SHUTTLE REENTRY SIMULATION CAPABILITY

- SIMULATION OF 1500-7100 NMI TRAJECTORY
- SIMULATION OF HIGH VELOCITY (25 KFT/SEC) TRAJECTORIES
- SIMULATION OF FLAT REENTRIES (LOW ENTRY ANGLES)
- MULTIPLE PAYLOADS
  - RV'S
  - BUSES
  - SITE DEFENSE RADAR TARGETS
- IMPACT AREA SELECTION FLEXIBILITY
  - WEATHER EFFECTS
  - TERMINAL GUIDANCE OVER LAND
  - RANGE SAFETY PROBLEMS REDUCED

FIGURE 24

TYPICAL DOD EXPERIMENT MISSION

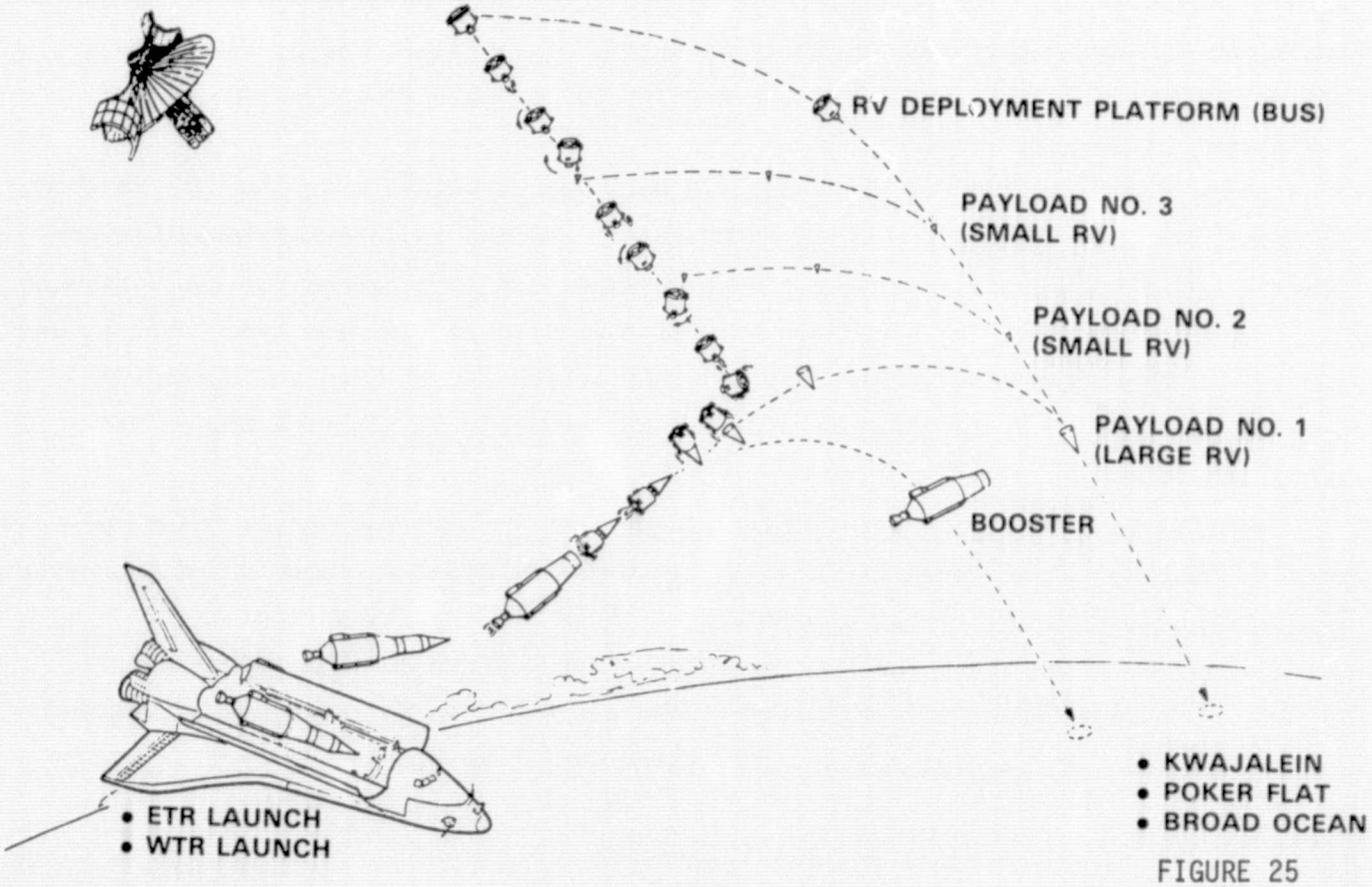

FIGURE 25

APPROACH CORRIDORS TO KREMS RADARS

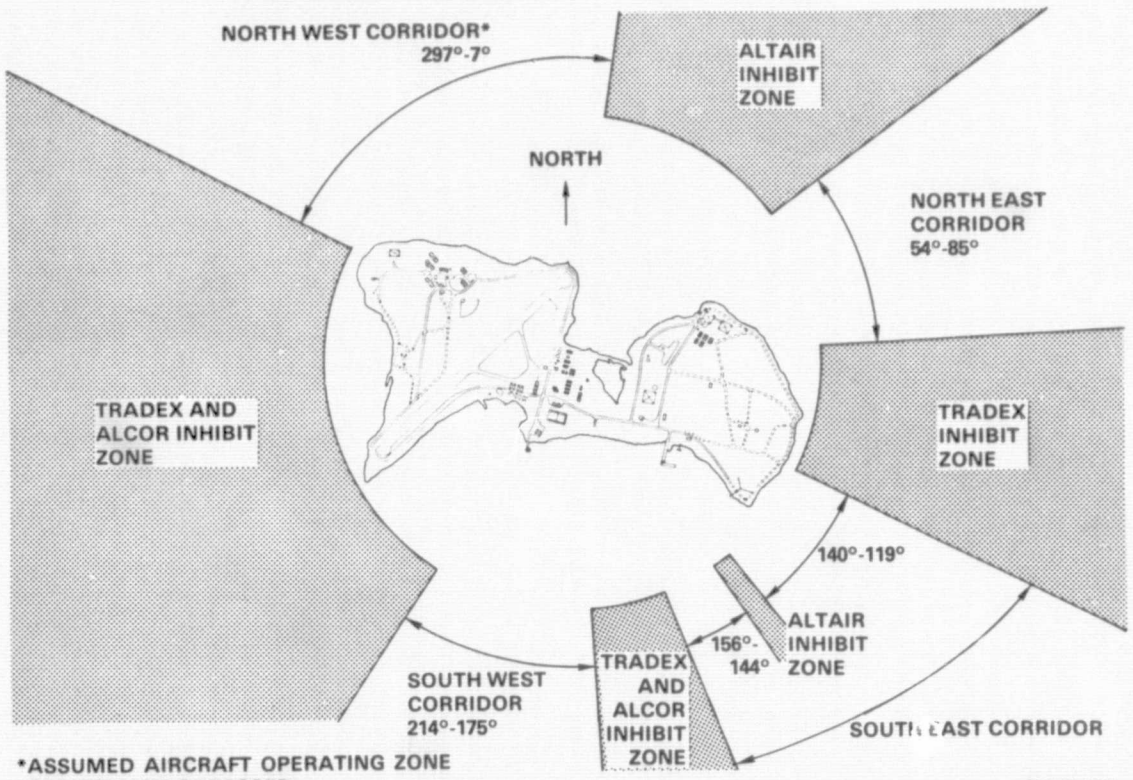

*ASSUMED AIRCRAFT OPERATING ZONE RESTRICTION BYPASSED.

FIGURE 26

LOCATION OF IMPACT POINT FOR SOUTHWEST APPROACH TO KWAJALEIN

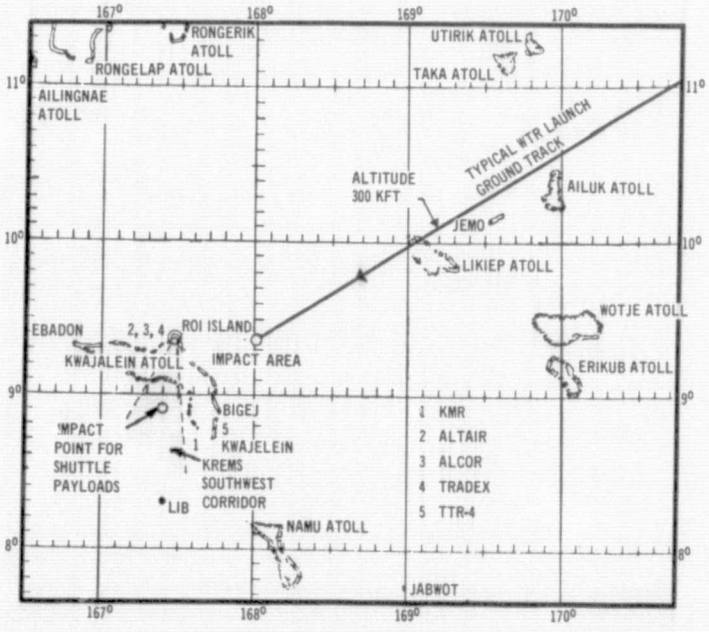

FIGURE 27

POKER FLAT FLIGHT ZONES 2, 3 & 4

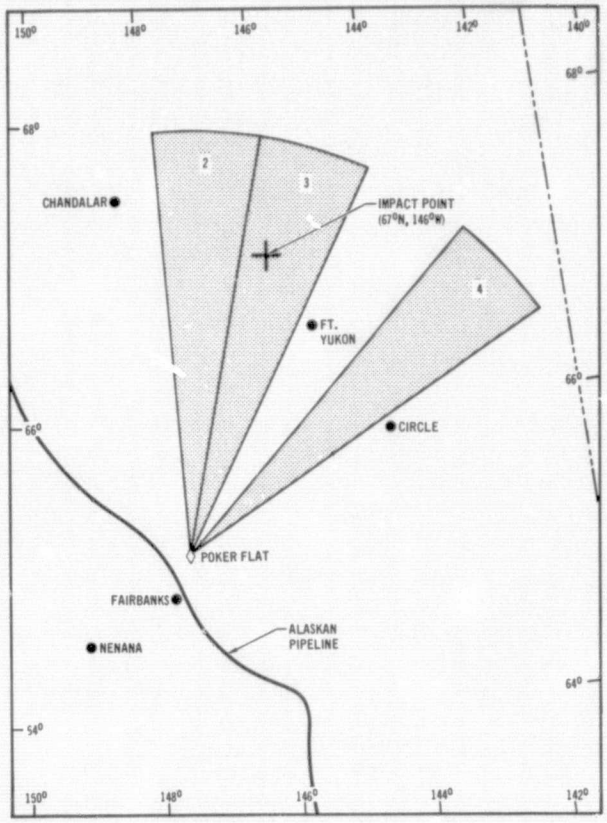

FIGURE 28

OPTIMUM BROAD OCEAN AREA SELECTION – STRATEGY

LAUNCH FROM KENNEDY SPACE CENTER

INCLINATION – 30° INCLINATION

ORBIT ALTITUDE – 160 NMI ORBIT ALTITUDE

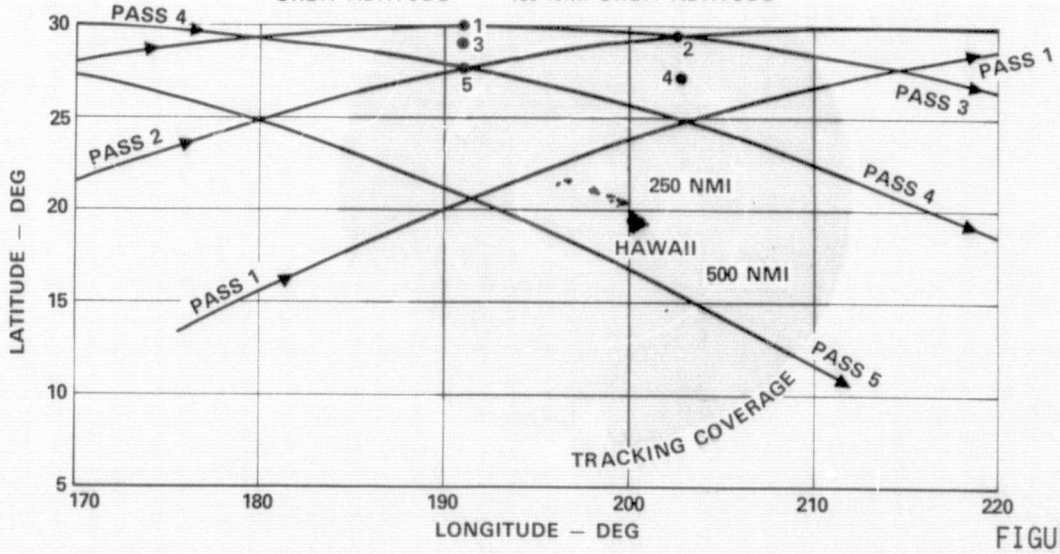

FIGURE 29

of Hawaii are identified by numbers 1-5 in Figure 29. The numbers correspond to the number of consecutive opportunities with minimum plane change ΔV requirements. Figure 30 summarizes the Shuttle orbit inclination and number best suited for payload impact at KMR, Poker Flat, and Hawaii. Note that impact at any three of the areas can be achieved by either a KSC or VAFB launch.

Shuttle Payloads can Achieve a Wide Range of Reentry Conditions at High Velocity To help identify the range of reentry velocities and flight path angles for which a large booster, e.g., Centaur, could be used, Figure 31 is presented. The left chart is for delivery of 8 RV's weighing 200 lb spaced 90 seconds apart at the pierce point. Any reentry flight path angle-velocity combination within the shaded area is achievable. Transtage can provide a small region of high velocity-shallow flight path reentries. On the other hand, Centaur can provide a large area of the V-γ map. These areas are compared with the Atlas ground launch from VAFB to KMR for the same number and spacing of payloads. Because of the fixed range from launch to impact, the Atlas capability is a line and not an area. Shuttle delivered payloads can achieve a wider range of reentry conditions and, in addition, higher reentry velocities compared to a typical ground launch.

High Velocity-Shallow Flight Path Angle Reentries are Shuttles Forte' - Because the Shuttle is in a circular orbit with velocities near 25 kft/sec, it takes little booster energy to deorbit a payload from the Shuttle orbit at these velocities and shallow flight path angles. The single 1000-lb RV capability, shown on the right hand chart of Figure 31, demonstrates the capabilities of medium and small boosters. Transtage and the Minibus concept (a small booster assembled from Shuttle RCS components) are compared. The Transtage can achieve a wide range of reentry conditions at high velocity indicating that it is oversized for much of the conditions. The Minibus is designed specifically to provide high velocity-shallow flight path angle reentry conditions. Note that the Atlas F can also provide specific reentry conditions over the same range as Transtage and has additional capability at steep flight path angles. However, the fixed range constraint still applies. The advantage of Shuttle for these reentry conditions is the capability to achieve payload reentry at other impact points such as Poker Flat and Hawaii.

Simulation of the Exoatmospheric Trajectory is Provided - A preferred payload deorbit procedure which provides maximum exoatmospheric payload trajectory simulation as well as minimal time between PDS* deployment from Shuttle and payload impact is described in Figure 32. This strategy involves deploying the PDS from

*PDS = Payload Deployment System

PREFERRED ORBITS FOR PDS DEORBIT (160 NMI SHUTTLE ORBIT ALTITUDE)

LAUNCH SITE	IMPACT AREA	SHUTTLE ORBIT INCLINATION (DEG)	PREFERRED ORBITS FOR DEORBIT
KSC	KMR	57	4, 5, 12, 13
	POKER FLAT	57	5, 6
	HAWAII	30	1 - 6
VAFB	KMR	72	4, 5, 13, 14
	KMR	90	3, 4, 11, 12
	POKER FLAT	72	2, 12, 13
	POKER FLAT	90	1, 2, 9, 10

FIGURE 30

HIGH VELOCITY & SHALLOW REENTRY ANGLES EASILY SIMULATED BY SHUTTLE/PDS DELIVERY

[IMPROVES UPON GROUND LAUNCH CAPABILITIES]

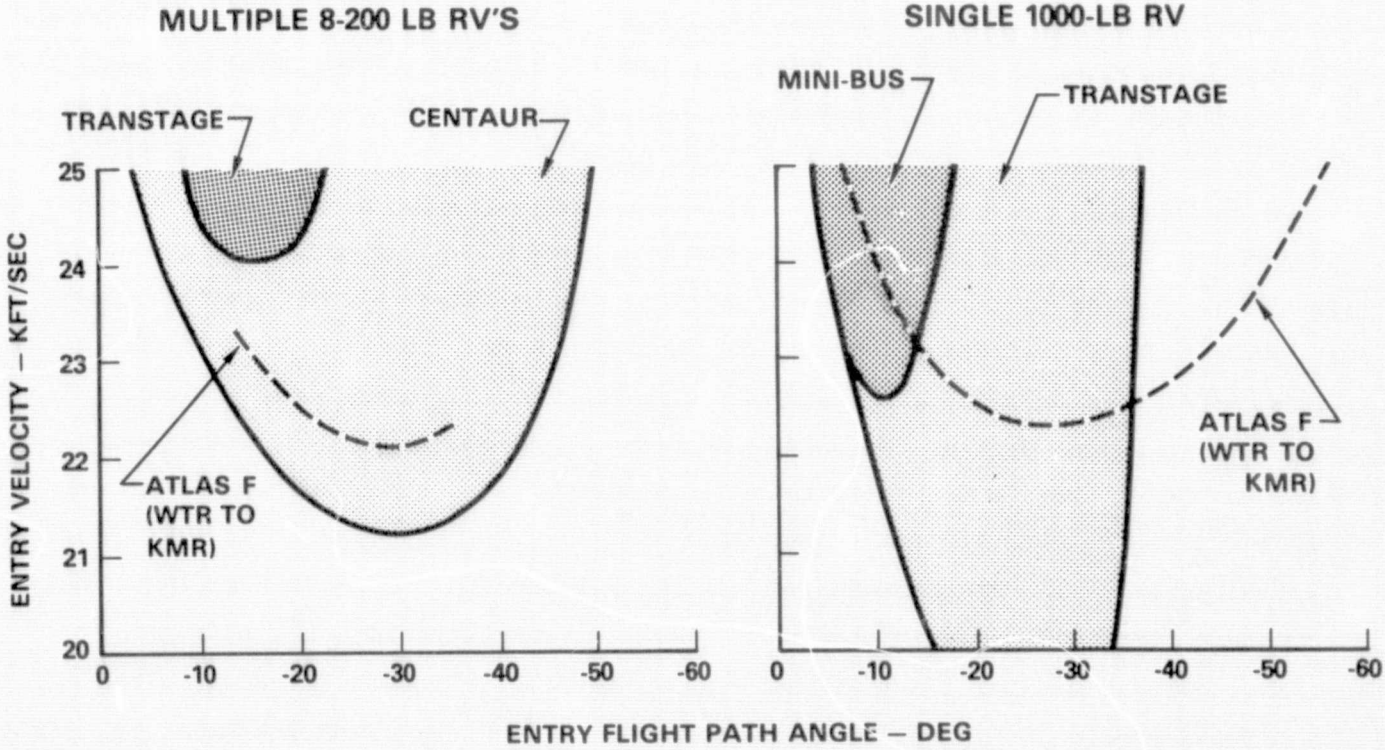

NOTE: 90 SEC SPACING AT PIERCE

FIGURE 31

SHUTTLE/PDS MANEUVER STRATEGY STUDIES HAVE IDENTIFIED UNIQUE CAPABILITIES

DEORBIT

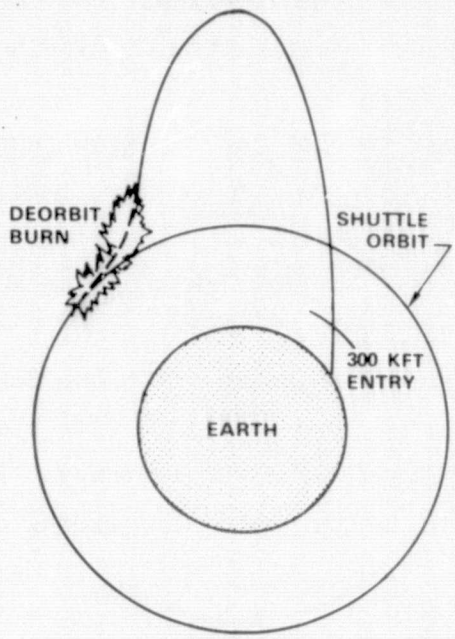

- ALLOWS TRAJECTORY RANGE SIMULATIONS OF 1500-7100 NMI

PLANE CHANGE

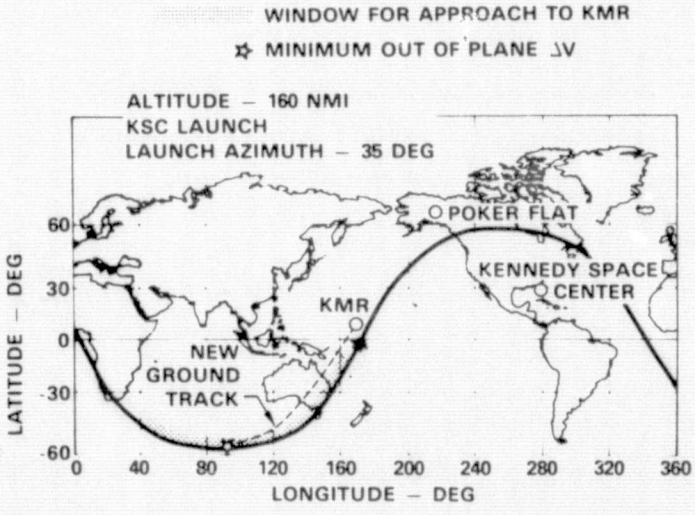

- PROVIDES FULL KREMS COVERAGE
- PROVIDES MULTIPLE PASS DEORBIT OPPORTUNITIES AT KWAJALEIN, HAWAII & POKER FLAT

PAYLOAD SPACING

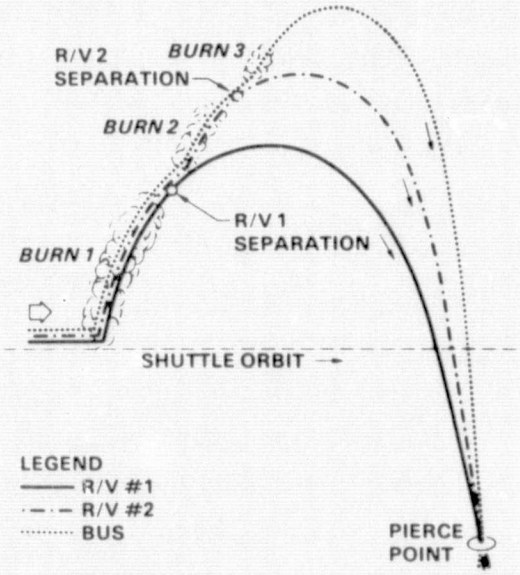

- IMPROVES UPON MULTIPLE PAYLOAD NUMBER & WEIGHT OF GROUND LAUNCH SYSTEMS

FIGURE 32

Shuttle; the PDS then performs a plane change maneuver to target it for the impact point; a deorbit burn is then made to place the PDS on the upleg of a ballistic reentry trajectory; spacing burns (analogous to ground launch procedure) follow to provide the desired payload spacing at the pierce point. Because the PDS deorbit maneuver can be initiated at any point on a Shuttle orbit, the simulation of 1500-7100 NMI trajectories is possible.

A Transtage Class Booster can Meet Many of the DoD Reentry Requirements - Multiple burns are needed for the typical DoD mission. An existing storable booster best meets this requirement. The Transtage was selected from the booster candidates shown in Figure 33 as the example design for this booster class on the basis that it provides maximum performance capability with minimum modification. The relatively short length of less than 15 feet provides efficient packaging in the Shuttle payload bay and considerable space for additional payload sharing. This class of booster has a wide range of applicability to DoD mission requirements. Its compactness, multiple burns capability, and payload capacity, make it a strong candidate for the PDS booster.

Booster Total Impulse Requirements are Minimal for Many Missions - The performance data for Transtage can be plotted as a function of total impulse required. To some extent this provides the ability to consider other booster systems of comparable total impulse for these missions. Figure 34 presents the total weight of equal weight payloads as a function of total impulse required for 1, 2 or 4 payloads and the Transtage booster. The first payload reenters at 25 kft/sec and the flight path angles of -5, -10, -20 or -30 deg as identified on the figure. For shallow flight path angle missions, and payloads of 1000 lb, boosters with half the total impulse of Transtage will suffice.

The Payload Deployment System Consists of a Booster, Spin Separation System and RV's - An existing storable booster and proven spin separation system will minimize development cost and risk of the PDS and fulfill many of the DoD needs. In special cases requiring only one plane change and a large deorbit burn, a rocket motor booster could suffice. Figure 35 provides a comparison between the proposed SRM IUS and Transtage PDS. Both are nearly the same size and weight. The SRM IUS as shown is limited to two burn missions.

A Minibus Concept is More Efficient for Many DoD Missions - The Minibus concept was studied as an alternate to using the heavier Transtage for deploying the lighter,

BOOSTER CANDIDATES

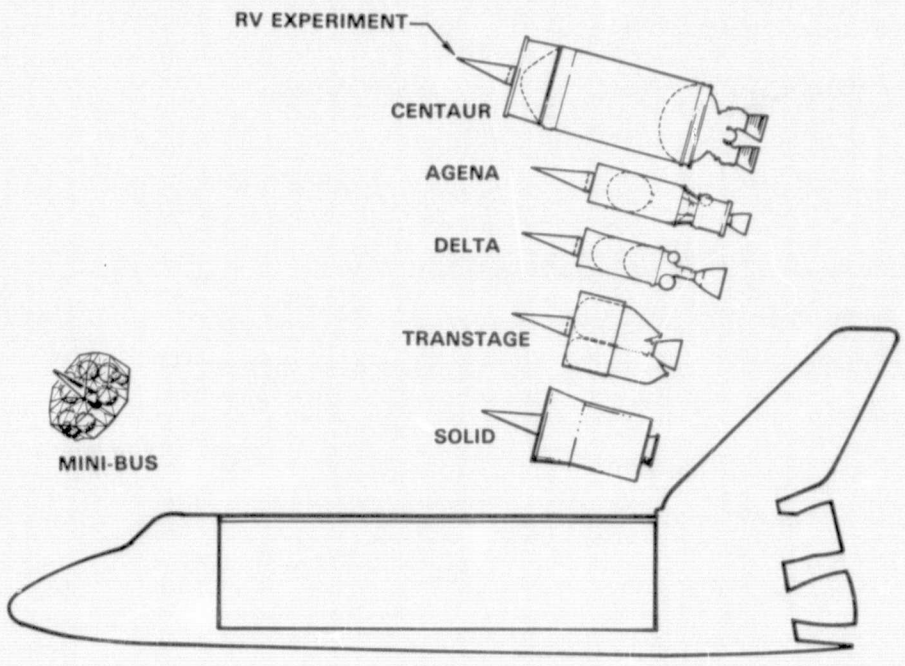

FIGURE 33

TRANSTAGE PERFORMANCE PARAMETRIC – TOTAL WEIGHT OF PAYLOADS

- o RELATIVE V_E = 25000 FT/SEC
- o 5000 FPS ΔV RESERVE

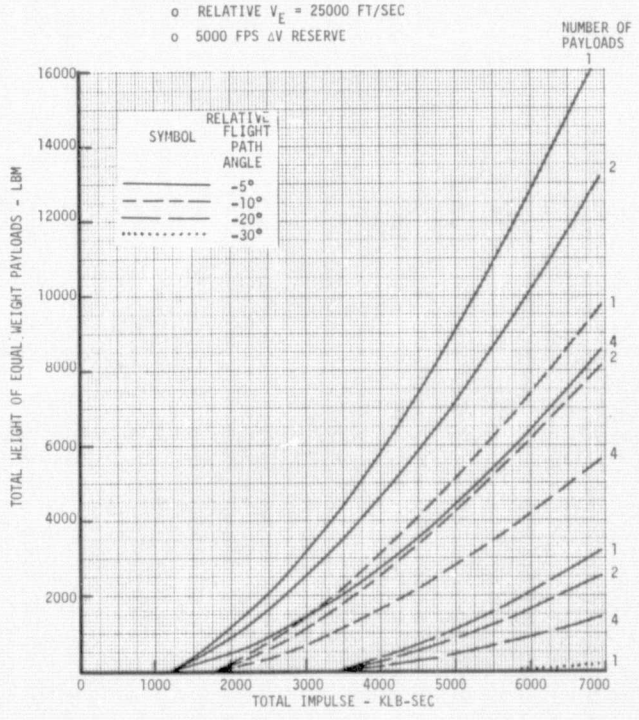

FIGURE 34

COMPATIBILITY OF RV INSTALLATION WITH SRM IUS & TRANSTAGE

SOLID ROCKET MOTOR (SRM) IUS

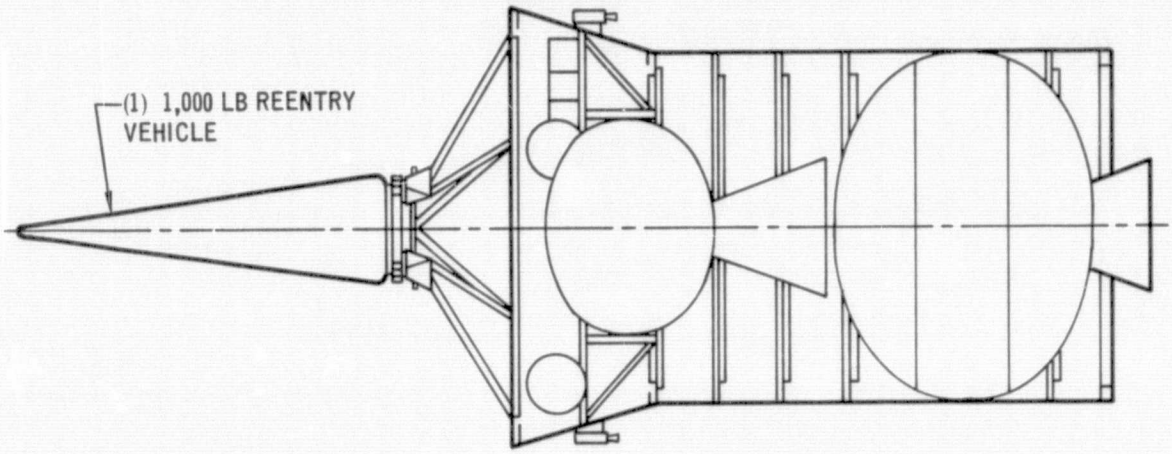

TRANSTAGE

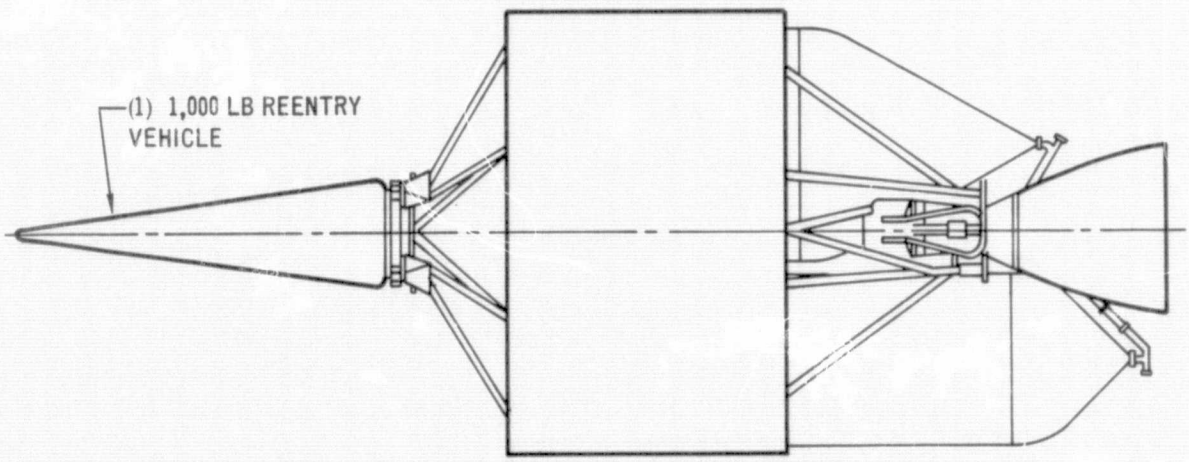

FIGURE 35

low ΔV reentry experiments. The configurations are made up of modules configured from the Shuttle Reaction Control System (RCS) components including the propellant, pressurization and engine systems. By combining several of these modules, higher total impulse is obtained. One such concept is shown in Figure 36. The RCS components were selected because (1) they will be fully qualified to all Shuttle requirements and hence have no development risk, (2) they will be fully compatible with all Shuttle flight, ground and maintenance requirements and equipment, and (3) they will be the newest and hence latest state of the art propulsion components from a performance standpoint.

The Minibus Maximizes the Length of Shuttle Payload Bay Available for Shared Payloads - The resulting packaging in the Shuttle payload bay for the Minibus concept and the Transtage are shown in Figure 37. The remaining lengths for shared payloads are 51 and 36-ft for the Minibus and Transtage, respectively. Also shown on the figure is the relative launch cost (not including payload, mission control or range costs) using the Minibus and a Transtage. A rather simple costing procedure based on used cargo bay volume shows the advantage of the Minibus. The recurring cost for the Minibus would be less than the Transtage and hence the launch cost is relatively low for the Minibus.

The PDS May Require a PDS to Satellite to Ground Data Link - If available Shuttle equipment is to be used for payload checkout, then the maximum data rate from each payload should not exceed 64 KBPS and preferably be less than 16 KBPS. Where higher payload data rates are necessary, checkout will require either a separate onboard checkout console or the data must be transmitted to the ground via one of Shuttle's wide band data links. In the latter case, ground personnel will evaluate the payload status and relay the information to the crew. Transmission of data directly to ground from separated payloads requires standard (5 watts) transmitters and flush-mounted, omni-directional antennas. Communication via TDRS, demonstrated for a NASA experiment in Figure 38, will require high power (50 watt) transmitters and steerable, directional antennas. This TDRS link may be required for range safety purposes since many of the PDS maneuvers will be made without ground tracking coverage. Command uplinks may also require satellite relay. Shuttle's ability to communicate with a separated payload is limited to about 20 NMI but it can radar track to 300 NMI, if the payload is equipped with a transponder.

A Shuttle Onboard Checkout Console for DoD Payloads May be Desirable - A block diagram of an Operation and Checkout Console is shown in Figure 39. PCM data enters the bit synchronizer where jitter is removed and a clock and data signal produced

MINIBUS CONCEPT (RCS DERIVATIVE 3)

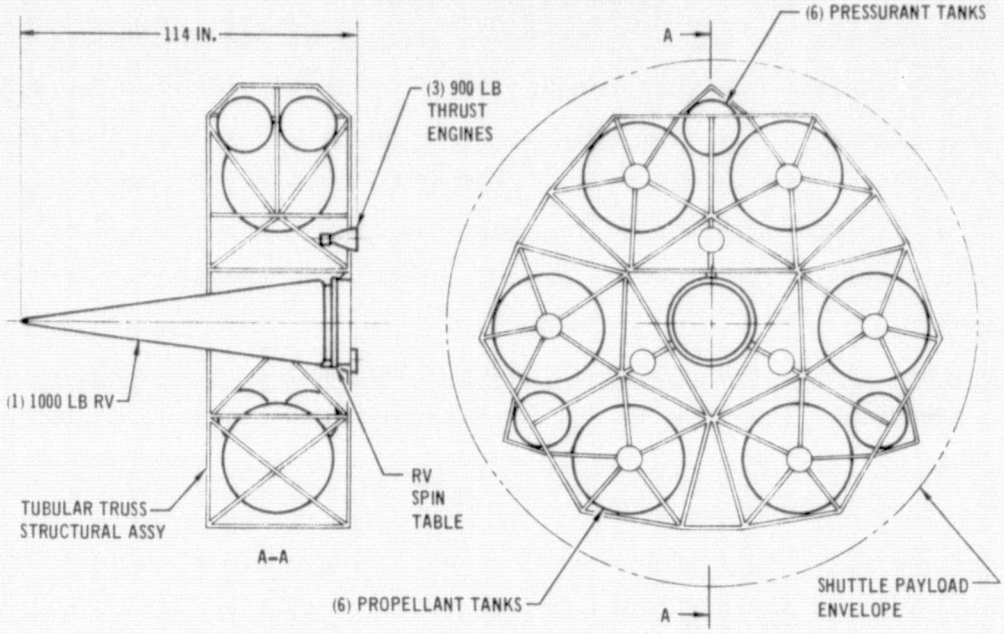

FIGURE 36

COMPARISON OF MINIBUS AND TRANSTAGE SHUTTLE PAYLOAD BAY UTILIZATION

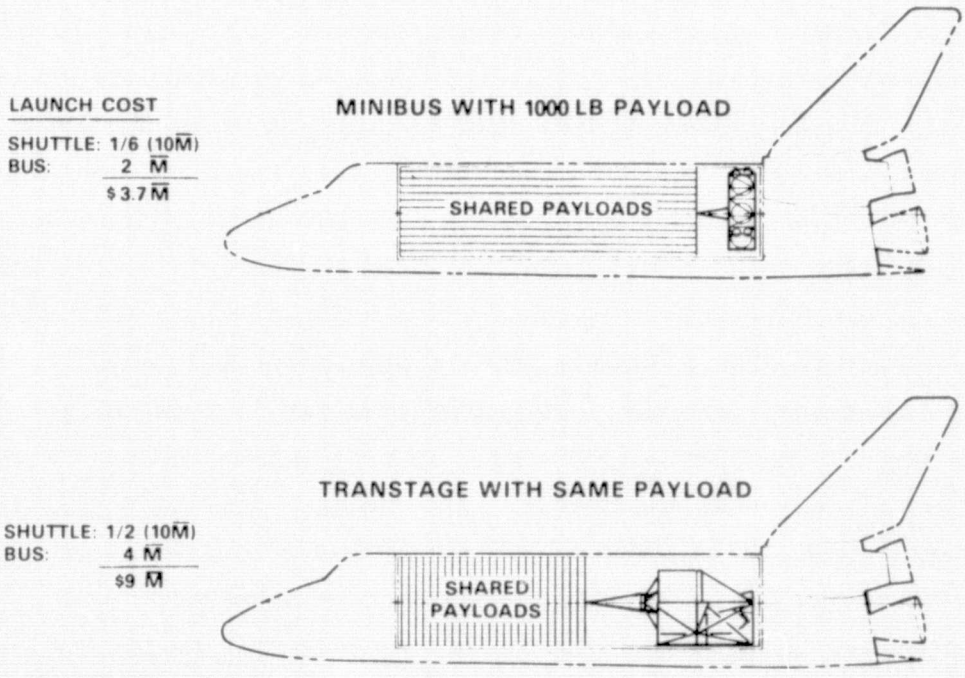

NOTE: 1971 DOLLARS

FIGURE 37

CURRENT ON-ORBIT SHUTTLE COMMUNICATION CAPABILITY

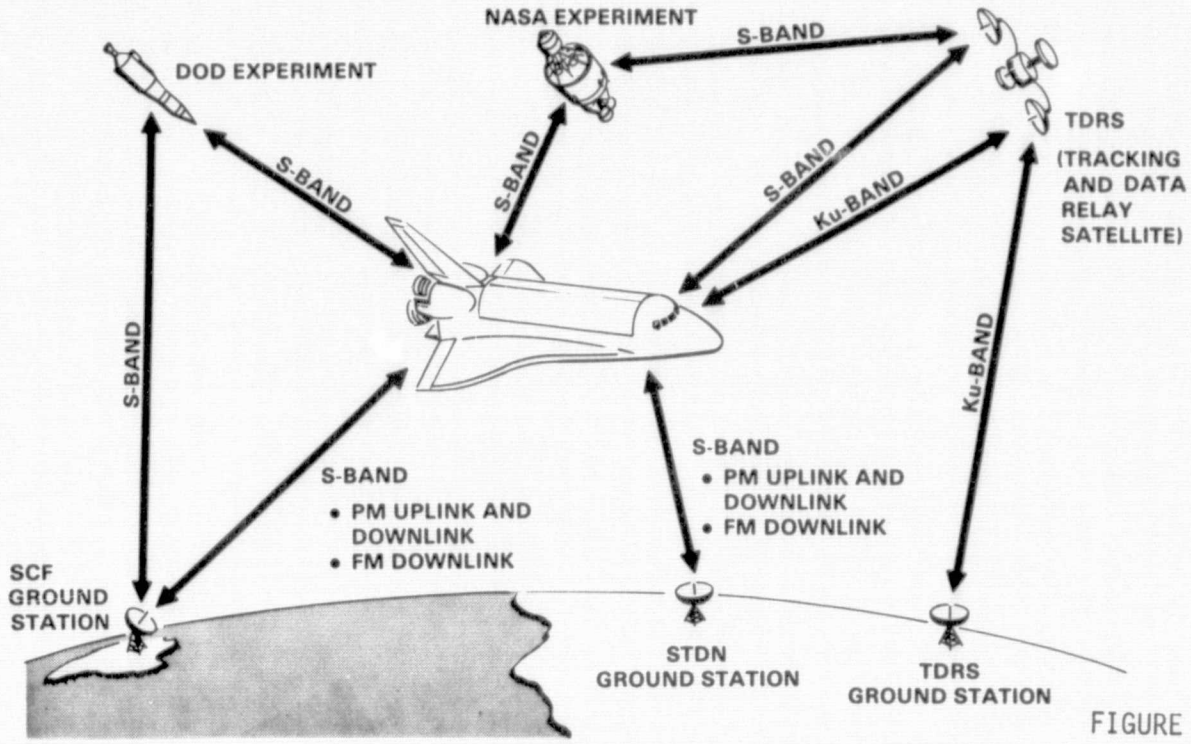

FIGURE 38

SHUTTLE PAYLOAD OPERATION AND CHECKOUT CONSOLE

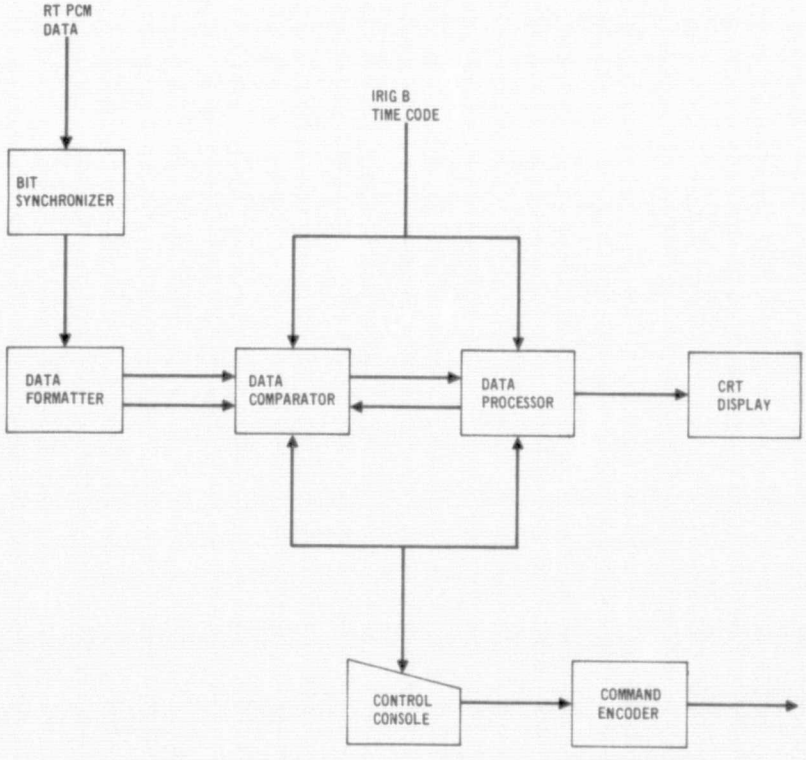

FIGURE 39

that is compatible with the data formatter input. The data formatter converts the serial digital data into parallel data words and adds a format location tag. The block diagram assumes all input data coming from a single source. This is compatible with the concept that the RV data is being interleaved in the PDS and is being sent over a high rate data link to a ground station for back-up processing. If this is not done, the data signals can be sent to the checkout console individually and selected either manually or automatically. If data from multiple RV's is to be intermixed during processing (a mixed source display is required), then a bit synchronizer and data formatter will be required for each data source.

An RV Cooling System is Required During Pre-Deployment Checkout - Current ground launched reentry technology experiments are powered-up for approximately ten hours prior to launch and cooled by air conditioning. Missions involving KSC launched experiments that reenter at Kwajalein are air borne for 6 hours for a 4 orbit mission compared to 30 minutes in space for a current ground launch. Missions from VAFB may be air borne as long as 21 hours. The Shuttle has primary and secondary heat exchange connectors up forward in the cargo bay to dissipate payload heat during Shuttle orbit. Passive, semi-active and active cooling systems may be installed on the payloads and interfaced with the payload heat exchangers. A heat sink/insulated vehicle, heat pipes, and internal RV water loop are recommended concepts described in Figure 40.

The Poker Flat Mission is Readily Accomplished by Shuttle Deployed Payloads - Shuttle capability to perform the example cases specified in Figure 41 are summarized in Figure 42. In cases 1 and 6 a combined plane change and deorbit burn was identified indicating application for a single burn SRM. For case 2 and 3 only one deorbit opportunity was established; a second opportunity would require approximately 10,000 fps plane change. Cases 4 and 5 are achievable from either VAFB or KSC with multiple opportunities on consecutive orbits. Total ΔV requirements are small for most missions The most severe ΔV requirement exists for the first opportunity of the first case. Only 20% of the Transtage propellant needs offloaded. However, by taking advantage of the combined burn over 42% offloading can be achieved. At the other extreme over 89% offloading is required for a case 4 launch from VAFB and a second opportunity deorbit. In fact for cases 2 through 5 a Minibus concept could perform these missions with much lower initial PDS mass and length. Mission 4 and 5 with impact at Poker Flat can be performed by either a KSC or VAFB launch with multiple deorbit opportunities, and small boosters of the Minibus class.

RECOMMENDED HEAT REJECTION SYSTEMS

CONCEPT 1 - RADIATOR WITH PCM

- o RV COVERED WITH RF TRANSPARENT ASTROQUARTZ (α/ε = .25)
- o HEAT SINK SUPPLEMENTED WITH PCM
- o ATTITUDE CONSTRAINTS FOR LONGER THAN NOMINAL MISSION DURATION

CONCEPT 2 - HEAT PIPE

- o HEAT PIPES ATTACHED TO HIGH HEAT REJECTION RV EQUIPMENT
- o CONTACT CONDUCTANCE TO BOOSTER USING PNEUMATIC LOADED PLATE
- o DECOUPLE BEFORE SPINUP BY RELEASING GAS PRESSURE

CONCEPT 3 - WATER COOLED RV EQUIPMENT

- o COLDPLATE HIGH HEAT REJECTION RV EQUIPMENT
- o QUICK DISCONNECT WATER LINES MECHANICALLY DECOUPLED PRIOR TO SPIN UP

FIGURE 40

SIX EXAMPLE CASES FOR SPECIFIC MISSION ANALYSIS

CASE NUMBER	REENTRY VEHICLE		PENETRATION AIDS		REENTRY CONDITIONS			
	NUMBER	WEIGHT-LB(EACH)	NUMBER	WEIGHT-LB(EACH)	γ DEGREES	V_E FT/SEC	SPACING (SEC)	IMPACT RANGE
1	1	600	1	30	28	22500	90*	KWAJALEIN
2	1	1000	-	-	5	25000	-	KWAJALEIN
3	2	1000	-	-	5	25000	90*	KWAJALEIN
4	1	1000	-	-	5	25000	-	POKER FLAT
5	2	1000	-	-	5	25000	90*	POKER FLAT
6**	2	350	4	30	28	22500	**	MECK ISLAND

*OR IDENTIFY MAXIMUM POSSIBLE SPACING IF 90 SEC CANNOT BE ACHIEVED BY TRANSTAGE

**VARIABLE IN TIME AND CROSSRANGE

FIGURE 41

SUMMARY OF EXAMPLE CASE RESULTS

CASE	OPPORTUNITY	LAUNCH SITE	IMPACT AREA	SHUTTLE ORBIT #	SHUTTLE ORBIT INCLINATION(DEG)	TRANSTAGE TOTAL ΔV (FPS)	% OFFLOAD
1	FIRST	KSC	KMR	4	57	15772	20
	COMBINED BURN			4		13338	42
2	FIRST	KSC	KMR	4	57	5416	84
3	FIRST	KSC	KMR	4	57	6047	78
4	KSC-1ST	KSC	PF	5	57	9369	65
	-2ND			6		8087	72
	VAFB-1ST	VAFB		12	72	4639	87
	-2ND			13		3928	89
	-3RD			14		4427	87
5	KSC-1ST	KSC	PF	5	57	10144	53
	-2ND			6		8806	62
	VAFB-1ST	VAFB		12	72	5505	81
	-2ND			13		4664	85
	-3RD			14		5147	82
6	COMBINED BURN	VAFB	MECK	3	90	11810	46

FIGURE 42

DoD Mission Sequence is Easily Accommodated by Shuttle - A typical mission sequence is shown in Figure 43. From the time of Shuttle launch at point 1 to achievement of circular orbit is almost one full orbit. The PDS deployment occurs at the end of the third orbit over the Pacific. By the time the PDS passes over Canada it is ready for the plane change maneuver at point 4. As it approaches the coast of Africa the deorbit burn is completed, the RV deployed, and the spacing burn performed. Approximately 40 minutes later the RV reenters at KMR. Six hours after Shuttle launch the payload impacts at KMR. These time lines may vary depending upon specific launch conditions and deorbit requirements, but the mission sequence seems to allow sufficient time for all prelaunch checkout and commit decision to be made.

Pierce Point Dispersion Very Sensitive to Shuttle Position and Velocity Tracking Errors - Accuracy of the pierce point location suffers because of tracking errors in Shuttle location and velocity. The downrange error in Shuttle velocity can result in pierce point downrange dispersions as large as 6.4 NMI per ft/sec velocity error for the shallow flight path angle reentries. By providing Shuttle tracking updates just prior to PDS deployment this error can be significantly reduced. Otherwise impact points will have to be displaced from populated areas to account for the pierce point dispersions. This is a severe problem for shallow reentry missions. Methods of improving accuracy should receive high priority.

Shuttle Unique Costs are Checkout Console, PDS Transmitter, and RV Coolant System Related - The absolute cost of using Shuttle launches compared to ground launches is not defined in this study. In fact, overland flights into Poker Flat appear as a unique capability of Shuttle and, therefore, a comparison is unwarranted. Shuttle costs over and above traditional ground launches will involve primarily the communications aspects of the missions, i.e., checkout console, satellite or ship coverage during PDS burns, and special PDS equipment to interface with Shuttle data links. Figure 44 summarizes the three significant cost items for Shuttle launched DoD entry technology experiments, i.e., checkout console, PDS antenna, and RV cooling system. The total development cost is $1.5M and the unit costs $325K. The checkout console unit is reusable with reprogramming for each DoD mission and its recurring cost is $100K. These ROM cost estimates can be used with estimates of Shuttle launch and PDS booster costs to compare the total Shuttle mission costs with comparable ground launches.

SHUTTLE MISSION SEQUENCE FOR PAYLOAD IMPACT AT KWAJALEIN

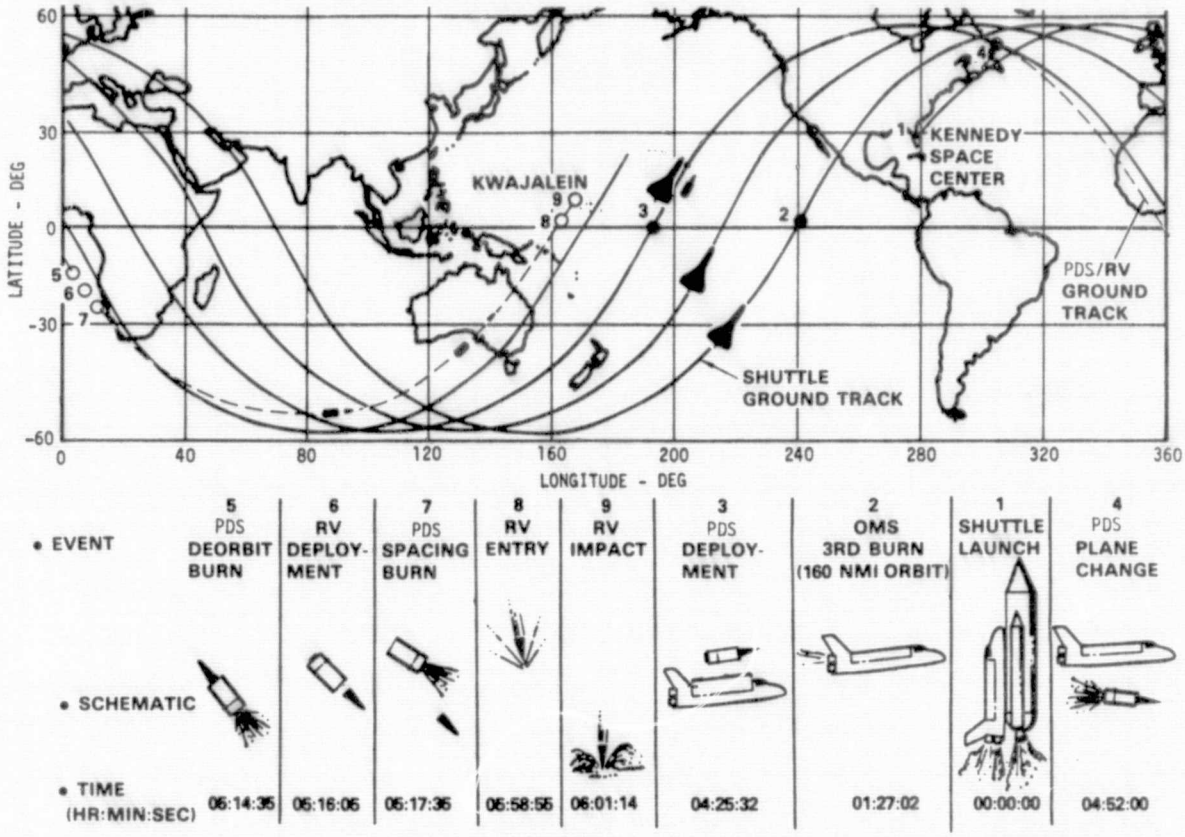

FIGURE 43

COST SUMMARY FOR DOD PAYLOADS

ITEM	DEVELOPMENT $K	UNIT $K	RECURRING $K
o CHECKOUT CONSOLE	900	250	100
o PDS TRANSMITTER	400	50	50
o COOLANT SYSTEM	200	25	25
TOTAL	1500	325	175

FIGURE 44

Now is the Time to Begin Design and Implementation Studies - Recommendations for additional studies, Shuttle, PDS, and RV equipment changes, and support equipment have been identified in this study. Seven areas requiring more detailed study are KMR range safety, KREMS ALTAIR-TRADEX interaction, Poker Flat range development, Minibus design, TDRSS usage, onboard checkout and improved targeting accuracy. The KMR range safety study should address the range safety considerations for the southwest corridor at KMR. The tracking coverage requirements should be defined from this study to enable detailed mission planning to be accomplished.

Investigation of the KREMS west-southwest corridor is required to define any problems involved with the TRADEX radiating at ALTAIR. If the TRADEX-ALTAIR interaction was found not to be a problem, the number of orbit opportunities at KMR would increase and the plane change requirements would be reduced.

A detailed mission study for delivering PGRV to Poker Flat is recommended to fully define the utility of the Poker Flat range and what modifications and instrumentation are necessary to support DoD missions. Because many of the DoD missions require a small deorbit booster of the Minibus class, design studies should be initiated to develop a design for use in the 1980's.

By defining the costs of services for using the TDRSS, comparisons with ship or Shuttle tracking could be made and a preferred PDS tracking network established. Design of checkout console hardware and software for pre-deployment checkout of the PDS is required.

As noted earlier, nearly an order of magnitude reduction in downrange dispersions is required to match desired system delivery accuracy.

Implementation of the above recommendations in the next few years will greatly reduce interface problems in the 1980's when DoD entry technology testing from Shuttle may be a reality. Early detailed studies and equipment development will provide an orderly transition to the use of Shuttle for some of the unique applications identified in this study.